

Pace in Concert with Phase:
Rate-induced Phase-tipping in Birhythmic Oscillators

Ravi Kumar K¹, Hassan Alkhayuon², Sebastian Wieczorek² and
Partha Sharathi Dutta^{1,*}[†]

¹Department of Mathematics
Indian Institute of Technology Ropar
Rupnagar, Punjab 140 001, India

²School of Mathematical Sciences
University College Cork
Cork T12 XF62, Ireland

arXiv:2502.09190v1 [math.DS] 13 Feb 2025

[†]Email: ravi.21maz0002@iitrpr.ac.in (Ravi Kumar K), hassan.alkhayuon@ucc.ie (Hassan Alkhayuon), sebastian.wieczorek@ucc.ie (Sebastian Wieczorek), *Corresponding author: parthasharathi@iitrpr.ac.in (Partha Sharathi Dutta)

Abstract

We study rate-induced phase-tipping (RP-tipping) between two stable limit cycles of a birhythmic oscillator. We say that such an oscillator RP-tips when a time variation of an input parameter preserves the bistability of the limit cycles but induces transitions from one stable limit cycle to the other, causing abrupt changes in the amplitude and frequency of the oscillations. Crucially, these transitions occur when: the rate of change of the input is in a certain interval bounded by *critical rate(s)*, and the system is in *certain phases* of the cycle.

We focus on two illustrative examples: the birhythmic van der Pol oscillator and the birhythmic Decroly-Goldbeter glycolysis model, each subjected to monotone and non-monotone shifts in their input parameters. We explain RP-tipping in terms of properties of the autonomous frozen system, including the *phase* of a cycle and *partial basin instability* along the parameter path traced by the changing input. We show that RP-tipping can occur as an irreversible one-way transition or as a series of transitions between the stable limit cycles. Finally, we present RP-tipping diagrams showing combinations of the rate and magnitude of parameter shifts and the phase of the oscillation that give rise to this genuine non-autonomous instability.

Keywords: RP-tipping, birhythmicity, time-dependent external input, non-autonomous systems, phase of a limit cycle, partial basin instability

1 Introduction

Critical transitions are nonlinear phenomena that can be understood as abrupt, significant, and unforeseen changes in the state of a dynamical system, often accompanied by crossing a tipping point due to minor and gradual changes in the external input (Scheffer 2009, Ashwin et al 2012). The notion of a tipping point was popularised by Gladwell (2000) and has since found applications in diverse fields like ecology (Scheffer et al 2001, Carpenter et al 2011, Dakos and Bascompte 2014, O’Brien et al 2023), climate science (Ashwin et al 2012, Ritchie et al 2021, Lenton et al 2008), and systems biology (Trefois et al 2015, Sarkar et al 2019). Given the potential for sudden and often irreversible changes in natural and human systems linked to these tipping points, it becomes crucial to identify and comprehend the underlying dynamical mechanisms that trigger such transitions. Based on the trigger mechanism, tipping points can be categorised into four types (Ashwin et al 2012, Halekotte and Feudel 2020): bifurcation-induced tipping (B-tipping), rate-induced tipping (R-tipping), noise-induced tipping (N-tipping), and shock-induced tipping (S-tipping)[†]. Furthermore, depending on the form of the *base state* from which the critical transition occurs, that is, the attractor for the *frozen system* with fixed-in-time external input, one can speak of partial-tipping or phase-tipping (P-tipping) from limit cycles (Alkhayuon and Ashwin 2018, Alkhayuon et al 2021), multi-frequency tipping (M-tipping) from quasiperiodic torus (Keane et al 2020), and fragmented-tipping (F-tipping) from spatial patterns (Bastiaansen et al 2022). In this paper, changing *external inputs* are represented by shifting *input parameters* in the oscillator models, and are sometimes referred to as *external forcing*.

In general, R-tipping occurs when the input parameter changes at rates that are both fast enough and optimal, so the system fails to track the *moving base state* (quasi-static attractor), crosses some *moving threshold* in the phase space, and transitions to an *alternative state*. In contrast to B-tipping, R-tipping can (and usually does) occur even though the changing input parameter does not cross any autonomous bifurcation points of the base state in a frozen system. Optimal rates mean that R-tipping may occur above some critical rate or between two critical rates of parameter change (O’Keeffe and Wieczorek 2020, Longo et al 2021, Ritchie et al 2023). The moving threshold can be a moving basin boundary (O’Keeffe and Wieczorek 2020) or a moving excitability quasi-threshold (O’Sullivan et al 2023). The alternative state can be long-lived (another attractor in a multi-

[†]In some sense, one can view N-tipping and S-tipping as special cases of R-tipping.

stable system) (Vanselow et al 2022, Chaparro-Pedraza 2021), or finite-time (a transient response in an excitable system) (O’Sullivan et al 2023, Kaur and Dutta 2022, Vanselow et al 2024). The identification of critical rates and the exploration of the outcomes when these rates are crossed hold significant importance in the study of natural and human systems (Wieczorek et al 2011, van der Bolt and van Nes 2021, Kaur and Dutta 2022, O’Sullivan et al 2023, Ritchie et al 2023). Most studies on R-tipping have considered sudden transitions from a stationary base state (a stable equilibrium) (Wieczorek et al 2023, Ritchie et al 2023). However, many complex systems (Mickens 1996, Goldbeter 1996) exhibit non-stationary base states such as stable limit cycles, tori, or even chaotic attractors. Sudden transitions from non-stationary base states have been less studied and understood (Alkhayuon and Ashwin 2018, Alkhayuon et al 2021, Ashwin and Newman 2021, Longo et al 2021, Dueñas et al 2023, Longo et al 2024).

P-tipping occurs in nonlinear systems with an oscillatory base state, when an external input causes the system to transition to an alternative state, but only from certain phases of the oscillations (Alkhayuon and Ashwin 2018, Alkhayuon et al 2021, Longo et al 2024). P-tipping stands for either partial tipping or phase tipping. Alkhayuon and Ashwin (2018) investigated the occurrence of R-tipping from a stable limit cycle using the framework of pullback attractors in non-autonomous systems with asymptotic parameter shifts. They provided an illustrative example where the pullback attractor of the system fails to track the moving limit cycle base state (quasistatic attractor) of the frozen system partially. In other words, some trajectories of the pullback attractor diverge while others track the moving limit cycle base state. Crucially, this is a typical scenario for loss of tracking of moving non-stationary base states. Thus, this phenomenon was called *partial tipping* in Alkhayuon and Ashwin (2018). In an alternative approach, Longo et al. (Longo et al 2021, 2024) and Dueñas et al. (Dueñas et al 2023) studied the concept of partial tipping on the hull of a non-autonomous scalar ordinary differential equation. Recently, Alkhayuon et al (2021) studied tipping from a stable predator-prey limit cycle to an extinction equilibrium in two paradigmatic non-autonomous predator-prey models with an Allee effect and a time-varying input in the form of (discontinuous) jumps in the growth rate of the prey. In this setting, the tipping depends purely on the phase of the cycle when the jump occurs. Hence, it was called *phase-tipping*.

RP-tipping is a combination of R-tipping and P-tipping in the sense that the system tips from an oscillatory base state if two conditions are satisfied simultaneously: (i) the rate of change of

the input is both fast enough and optimal, and (ii) the system state is in certain phases of the oscillatory base state.

One novelty of our work is that we explore RP-tipping from a base limit cycle to an alternative stable limit cycle. Such tipping implies a shift in the oscillation characteristics, e.g., amplitude and frequency. For example, an energy harvesting system exhibits the coexistence of two stable limit cycles in its wind-induced vibration (Kwuimy and Nataraj 2015, Zhang et al 2023). There, an undesired transition to the stable limit cycle with a smaller amplitude and different frequency results in less mechanical deformation and, consequently, less efficient conversion from wind to electrical energy. Here, we illustrate RP-tipping in two birhythmic oscillators: the birhythmic van der Pol oscillator (Kaiser and Eichwald 1991), which incorporates a higher-order polynomial damping factor, and the Decroly-Goldbeter glycolysis model of biochemical oscillations (Moran and Goldbeter 1984). Both systems exhibit a coexistence of two stable limit cycles separated by an unstable limit cycle, which is the defining feature of birhythmic oscillators (Goldbeter 1996, Biswas et al 2016).

To study RP-tipping in the aforementioned birhythmic oscillators, we subject these oscillators to monotone and non-monotone continuous time-dependent external inputs. Specifically, we consider parameter shifts (Ashwin et al 2017, Wieczorek et al 2021, Ritchie et al 2023) that do not cross any autonomous bifurcation points of the frozen system. In other words, there are always two stable limit cycles at any fixed level of the input parameter. The transitions between stable limit cycle attractors happen from certain phases, known as tipping phases. Hence, it is important to define the phase of the limit cycle explicitly. It is also essential to note that the inclusion of time-dependent external inputs makes the systems non-autonomous, meaning that the traditional autonomous bifurcation theory proves inadequate for exploring RP-tipping between stable limit cycles. Recent decades have witnessed the development of various methods (Kloeden and Rasmussen 2011, Ghil and Sciamarella 2023, Wieczorek et al 2021, 2023, Anagnostopoulou et al 2023) to study the dynamics of non-autonomous systems. One among these methods is "basin instability," which uses the geometric properties of the frozen autonomous system (O’Keeffe and Wieczorek 2020, Ritchie et al 2023). In Wieczorek et al (2023), the authors showed that the notion of basin instability provides easily verifiable sufficient conditions for the occurrence of R-tipping from equilibrium base states in higher dimensional nonlinear systems. Alkhayouon et al (2021) extended this

notion to "partial basin instability" to study P-tipping from oscillatory base states. In their work, partial basin instability of a stable limit cycle occurs by crossing the stable manifold of a saddle equilibrium, whereas, in our case, it happens by crossing the repelling limit cycle. We determine the region of partial basin instability of the coexisting stable limit cycles in their corresponding autonomous frozen system, and we identify appropriate parameter shifts that cause RP-tipping. In particular, we analyse two types of RP-tipping: one-way transitions and a series of alternating transitions between the two stable limit cycles.

We start with one-way transitions that can be interpreted as irreversible RP-tipping for both monotone and symmetric non-monotone parameter shifts. These transitions occur from the larger-amplitude base limit cycle to the smaller-amplitude alternative stable limit cycle in the birhythmic van der Pol oscillator, and conversely in the glycolysis model. We obtain two-dimensional RP-tipping diagrams with variations in the magnitude and rate of the parameter shifts. Depending on the model and the type of parameter shift, we observe either bounded or half-bounded RP-tipping regions, leading to the identification of two critical rates or one critical rate, respectively, for a given magnitude of the shift.

Next, we demonstrate a series of alternating transitions between both stable limit cycles in the birhythmic van der Pol oscillator with a non-monotone parameter shift in the form of an impulse. In this sequence, the system also transitions from the smaller-amplitude stable limit cycle to the larger-amplitude limit cycle and then back to the smaller-amplitude limit cycle.

The paper is organised as follows. Section 2 introduces two autonomous birhythmic oscillator models and identifies the coexistence of two stable limit cycles in each model using one- and two-parameter bifurcation diagrams, phase portraits, and the corresponding time series. Then, we set up the non-autonomous problem to study RP-tipping (subsection 2.3). In section 3, we define the phase of limit cycles and relate the concept of basin instability to the RP-tipping phenomenon. In section 4, we demonstrate RP-tipping in the birhythmic van der Pol model and the Decroly-Goldbeter glycolysis model. Finally, we summarise and conclude in section 5.

2 Mathematical models of birhythmic oscillators

In this section, we introduce the two distinct birhythmic oscillator models, identify the time-varying input parameters, and highlight limit cycle bistability in the corresponding frozen systems with

fixed-in-time input parameters.

2.1 Model 1: The birhythmic van der Pol model

The birhythmic van der Pol oscillator equation for a real variable x ,

$$\ddot{x} - \mu(1 - x^2 + \alpha x^4 - \beta x^6)\dot{x} + x + d(\dot{x} - x) = 0, \quad (1)$$

was introduced by Kaiser (Kaiser and Eichwald 1991), who modified the classical van der Pol oscillator equation with an additional higher-order polynomial damping factor $\mu(\alpha x^4 - \beta x^6)\dot{x}$. Later, Biswas et al (2016) included a new feedback term $d(\dot{x} - x)$. For our analysis, it is convenient to rewrite the second-order differential equation (1) as two coupled first-order differential equations:

$$\begin{cases} \dot{x} = y, \\ \dot{y} = \mu(1 - x^2 + \alpha x^4 - \beta x^6)y - x - d(y - x), \end{cases} \quad (2)$$

where $\mu > 0$ is the *external input parameter*, $\alpha > 0$ and $\beta > 0$ are non-linear damping parameters, and d is the feedback strength. In Ref. (Biswas et al 2016), the authors assumed that the periodic solutions of (1) can be approximated by $x(t) = A \cos(\omega t)$, where A is the amplitude and ω is the angular frequency of the oscillator, and then by employing the harmonic decomposition method they derived the following amplitude equation:

$$\mu \left(1 - \frac{1}{4}A^2 + \frac{\alpha}{8}A^4 - \frac{5\beta}{64}A^6 \right) - d = 0. \quad (3)$$

Equation (3) provides an approximate relationship between the system parameters and the oscillation amplitude. The number of roots of (3) for a given μ and d determines the number of possible periodic solutions to Eq. (1), (see Fig. 1 and Fig. 2(b)).

There is a range of parameters where (3) has three positive real roots. Two of these roots, namely $A_{\Gamma_1} > A_{\Gamma_2}$, correspond to two stable limit cycles Γ_1 and Γ_2 . The third root, namely A_θ , where $A_{\Gamma_1} > A_\theta > A_{\Gamma_2}$, corresponds to the unstable limit cycle θ . The time series for all three limit cycles are shown in Fig. 1.

To identify the range of parameters where all three limit cycles exist, we fix $\alpha = 0.093$ and

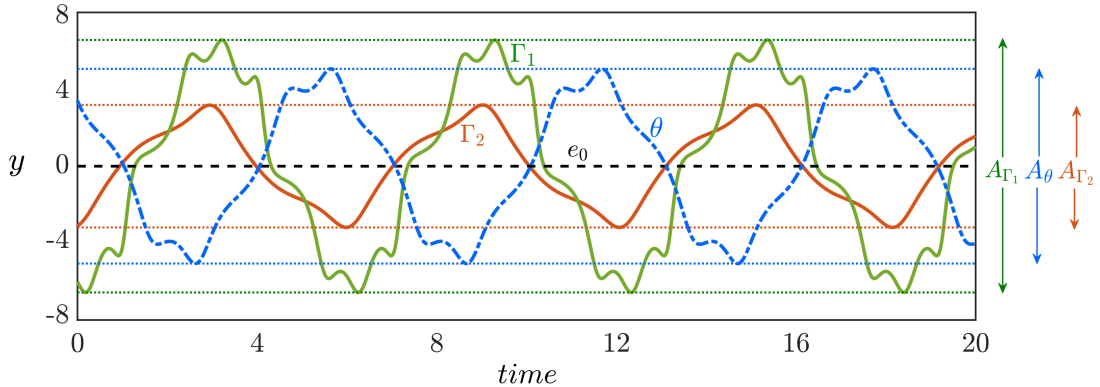


Figure 1. Time series of the birhythmic van der Pol oscillator (2) exhibiting limit cycle oscillations with different amplitudes and frequencies. The horizontal dotted lines indicate the maxima and minima of the large-amplitude stable limit cycle Γ_1 (green), the unstable limit cycle θ (blue), and the small-amplitude stable limit cycle Γ_2 (red) along with the amplitudes A_{Γ_1} , A_θ , and A_{Γ_2} (marked with double sided arrows), respectively. The dashed black line at $y = 0$ denotes an unstable equilibrium point e_0 . The parameter values are $d = -0.1$, $\alpha = 0.114$, $\beta = 0.003$, and $\mu = 0.6$.

$\beta = 0.0019$ and produce a two-parameter bifurcation diagram for the autonomous model (2) in the plane (d, μ) in Fig. 2(a). The bifurcation analyses have been performed using the *XPPAUT* package (Ermentrout 2002). In Fig. 2(a), the grey-shaded region-I marks the parameter region with three limit cycles. The maxima and minima for two stable and one unstable limit cycles are shown in the grey-shaded portion of the one-parameter bifurcation diagram in Fig. 2(b) for $d = -0.05$ (corresponding to the vertical dashed line in Fig. 2(a)). Depending on the chosen initial conditions, the system's trajectories converge towards either the large-amplitude (Γ_1) or the small-amplitude (Γ_2) stable limit cycle, represented by the green and red branches, respectively, in Fig. 2(b). The blue dashed branches represent the maxima and minima of the unstable limit cycle (θ), acting as a separatrix between the two stable limit cycles. Pairs of limit cycles collide and disappear at the fold (saddle-node) of limit cycles bifurcation points F_{l1} and F_{l2} . The dashed black line at $x = 0$ represents the unstable equilibrium e_0 .

To each side of the birhythmic region-I in Fig. 2(a), there is a monorhythmic region with a single small-amplitude stable limit cycle Γ_2 in region-II, or single large-amplitude stable limit cycle Γ_1 in region-IV. The small-amplitude stable limit cycle Γ_2 from region-II disappears along the supercritical Hopf bifurcation curve H , leaving just one stable equilibrium point e_0 in region-III. Examples of phase portraits in different regions from Fig. 2(a), including the cycles Γ_1 , Γ_2 , θ , and the equilibrium e_0 (stable in region-III and unstable in other regions), are shown in Fig. 3.

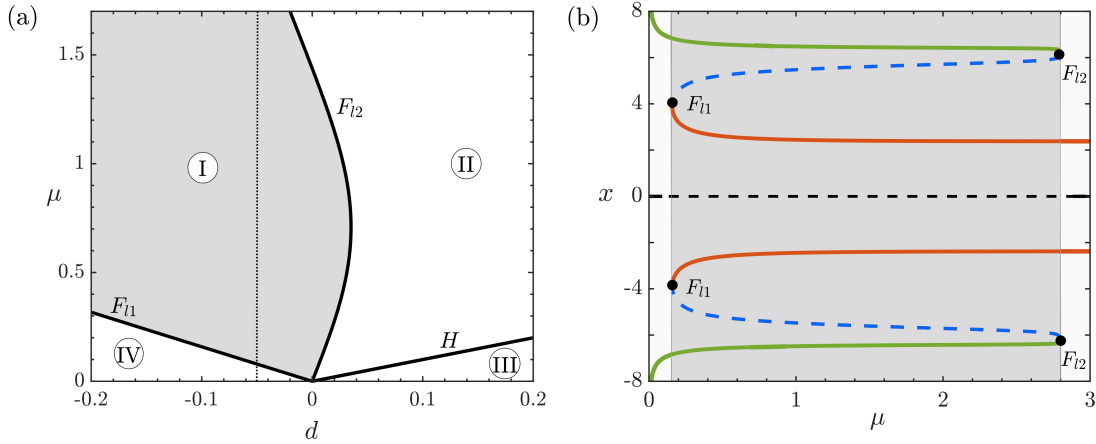


Figure 2. (a) Two-parameter bifurcation diagram of the birhythmic van der Pol oscillator (2) with variations in the parameters d and μ . F_{l1} , and F_{l2} represent the fold/saddle-node bifurcation of limit cycles (SNLC) curves where a stable limit cycle and an unstable limit cycle merge and disappear, and H represents the Hopf bifurcation curve. The grey-shaded region-I marks the coexistence of two stable limit cycles Γ_1 and Γ_2 (birhythmicity) separated by an unstable limit cycle θ ; in region-II, the small amplitude stable limit cycle Γ_2 exists alone (monorhythmicity); region-III marks the existence of a stable steady state (point attractor); and in region-IV, the large amplitude stable limit cycle Γ_1 exists alone (monorhythmicity). The vertical dotted line represents the value of $d = -0.05$ for which the one-parameter bifurcation diagram is plotted. (b) One-parameter bifurcation diagram exhibiting the maxima and minima of each limit cycle with variations in the parameter μ . The stable limit cycles are marked with solid (red and green) curves, and the unstable limit cycle is marked with a dashed (blue) curve. The dashed horizontal line at $x = 0$ represents an unstable equilibrium point. The grey-shaded region represents the existence of birhythmicity. Other parameter values are $\alpha = 0.093$, and $\beta = 0.0019$.

2.2 Model 2: The Decroly-Goldbeter glycolysis model

The Decroly-Goldbeter glycolysis model of enzyme reaction (Moran and Goldbeter 1984) in two real variables x (substrate) and y (product) is given by the following equations:

$$\begin{cases} \dot{x} = v + \frac{\sigma_i}{K^n + y^n} y^n - \sigma_M \Phi(x, y), \\ \dot{y} = q \sigma_M \Phi(x, y) - k_s y - q \frac{\sigma_i}{K^n + y^n} y^n. \end{cases} \quad (4)$$

Here, the parameter v is the constant input of substrate x , the *input parameter* σ_i is the normalized maximum rate of the recycling enzymes, σ_M is the normalized maximum rate of reaction, $q = M/K_p$, where M is the Michaelis constant and K_p denotes the dissociation constant of the product, and k_s is the removal rate of the product y . The term $\frac{\sigma_i}{K^n + y^n} y^n$ describes the feedback mechanism of the product into the substrate with the Hill coefficient $n \geq 3$ and the half-saturation constant

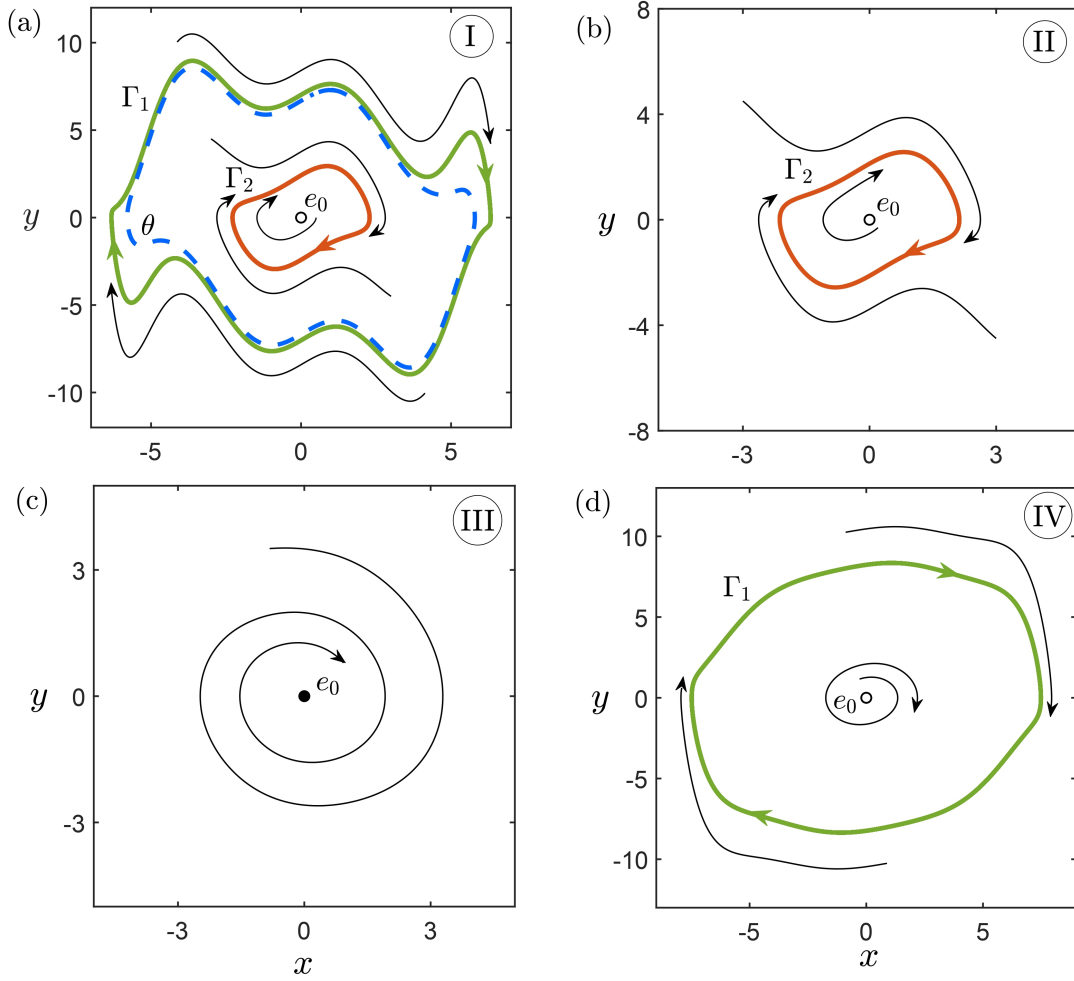


Figure 3. Phase portraits of the birhythmic van der Pol oscillator (2) corresponding to distinct regions shown in Fig. 2(a): For (a) $d = -0.001$ and $\mu = 1$ (region I: birhythmicity); (b) $d = 0.1$ and $\mu = 1$ (region II: monorhythmicity - small amplitude stable limit cycle Γ_2); (c) $d = 0.15$ and $\mu = 0.05$ (region III: stable equilibrium point); and (d) $d = -0.15$ and $\mu = 0.05$ (region IV: monorhythmicity - large amplitude stable limit cycle Γ_1). e_0 marked with an open circle stands for an unstable equilibrium point, and a filled circle stands for a stable equilibrium point. The blue dashed curve θ stands for the unstable limit cycle. The black curves headed with an arrow represent some exemplary trajectories. Other parameter values are same as in Fig. 2.

of the product K . The rate of reaction function is given as (Monod et al 1965):

$$\Phi(x, y) = \frac{x(1+x)(1+y)^2}{L + (1+x)^2(1+y)^2},$$

where L denotes the allosteric constant of the enzyme.

Fig. 4 shows the bifurcation structures of the autonomous model (4). The two-parameter bifurcation diagram (Fig. 4(a)) with variations in the parameters v and σ_i identifies four qualitatively different regions, where the grey-shaded region-I marks the coexistence of two stable and one un-

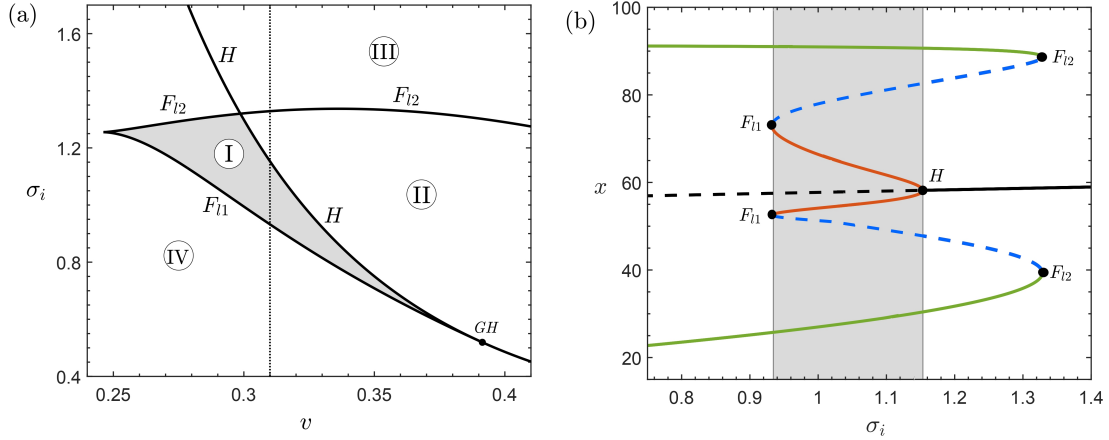


Figure 4. (a) Two-parameter bifurcation diagram of the Decroly-Goldbeter glycolysis model (4) with variations in the parameters v and σ_i . F_{l1} , and F_{l2} represent the SNLC curves where a stable limit cycle and an unstable limit cycle merge and disappear, and H represents the Hopf bifurcation curve. The filled circle marked by GH at $(v, \sigma_i) \approx (0.3914, 0.5195)$ represents the generalised Hopf (Bautin) bifurcation point where F_{l1} and H merge. The grey-shaded region-I marks the coexistence of two stable limit cycles Γ_1 and Γ_2 , separated by an unstable limit cycle θ ; in region-II, the large amplitude stable limit cycle Γ_1 coexists with a stable equilibrium point (hard-excitation); region-III marks the existence of a stable equilibrium point; and in region-IV, a single stable limit cycle exists. The vertical dotted line represents $v = 0.31$, for which the one-parameter bifurcation diagram is plotted. (b) One-parameter bifurcation diagram with variations in the input parameter σ_i . The maxima and minima of stable limit cycles are marked with solid (red and green) curves, and those of the unstable limit cycle are marked with dashed (blue) curves. The almost horizontal dashed (black) line represents an unstable equilibrium point, and the solid (black) line represents a stable equilibrium point. The grey-shaded region represents the existence of birhythmicity. Other parameter values are $K = 10$, $L = 3.6 \times 10^6$, $\sigma_M = 10$, $n = 5$, $q = 1$, and $k_s = 0.06$.

stable limit cycles. We denote the stable limit cycles with Γ_1 and Γ_2 , the unstable limit cycle with θ , and use the same colour coding as for the birhythmic van der Pol oscillator. Region-II presents hard excitation representing the coexistence of one stable limit cycle, one unstable limit cycle, and a stable equilibrium point, region-III marks the presence of a single stable equilibrium point, and region-IV denotes the existence of a single stable limit cycle. The region-I is bounded by one Hopf bifurcation curve H and two saddle-node bifurcations of limit cycle curves F_{l1} and F_{l2} . The maxima and minima for two stable and one unstable limit cycles are shown in the one-parameter bifurcation diagram in Fig. 4(b) for $v = 0.31$ (corresponding to the vertical dashed line in Fig. 4(a)). The grey-shaded region in Fig. 4(b) marks the coexistence of two stable and one unstable limit cycles.

Examples of phase portraits for different regions from Fig. 4(a), including the cycles Γ_1 , Γ_2 , θ , and the equilibrium e_0 , are shown in Fig. 5.

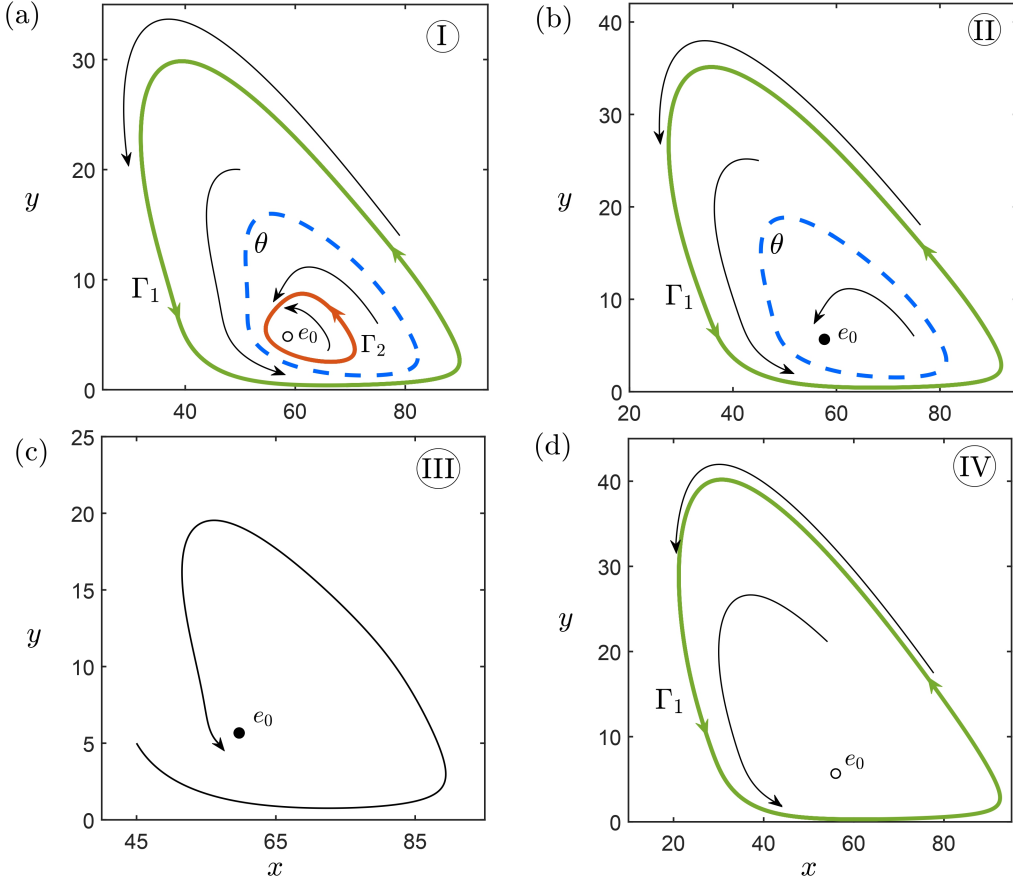


Figure 5. Phase portraits illustrating different dynamics of the Decroly-Goldbeter glycolysis model (4), corresponding to distinct regions as outlined in Fig. 4(a): For (a) $v = 0.29$ and $\sigma_i = 1.15$ (region I: birhythmicity); (b) $v = 0.34$ and $\sigma_i = 1.1$ (region II: hard excitation); (c) $v = 0.34$ and $\sigma_i = 1.6$ (region III: stable equilibrium point); and (d) $v = 0.34$ and $\sigma_i = 0.7$ (region IV: monorhythmicity). e_0 marked with an open circle stands for an unstable equilibrium point, and a filled circle stands for a stable equilibrium point. The blue dashed curve θ stands for the unstable limit cycle. The black curves headed with an arrow represent some exemplary trajectories. Other parameters are same as in Fig. 4.

2.3 Time-varying external inputs and non-autonomous models

In the remainder of the paper, we will analyse non-autonomous versions of models (2) and (4), where the external input parameters, μ and σ_i , are replaced with time-varying external inputs,

$$\mu(rt) \quad \text{and} \quad \sigma_i(rt),$$

respectively. Here, the *rate parameter* $r > 0$ quantifies the timescale of the varying external inputs. We will be interested in how the response of each birhythmic oscillator to its external input changes

as r is varied.

To simplify the discussion, we use $p(rt)$ to denote either $\mu(rt)$ or $\sigma_i(rt)$, and X to denote (x, y) from models (2) and (4). In other words, now each model can be written as:

$$\dot{X} = \frac{dX}{dt} = g(X, p(rt)). \quad (5)$$

Furthermore, we will consider bi-asymptotically constant external inputs (Wieczorek et al 2023), meaning that,

$$\lim_{t \rightarrow +\infty} p(rt) = p^+ \in \mathbb{R}, \quad \text{and} \quad \lim_{t \rightarrow -\infty} p(rt) = p^- \in \mathbb{R}. \quad (6)$$

To be specific, we consider monotone external input of the form:

$$p(rt) = \begin{cases} a - b \operatorname{sech}(r(t - t_c)) & \text{if } t \leq t_c, \\ a - b & \text{if } t > t_c, \end{cases} \quad (7)$$

and the corresponding non-monotone external input of the form:

$$p(rt) = a - b \operatorname{sech}(r(t - t_c)), \quad (8)$$

shown in Figs. 6(a) and 6(b), respectively.

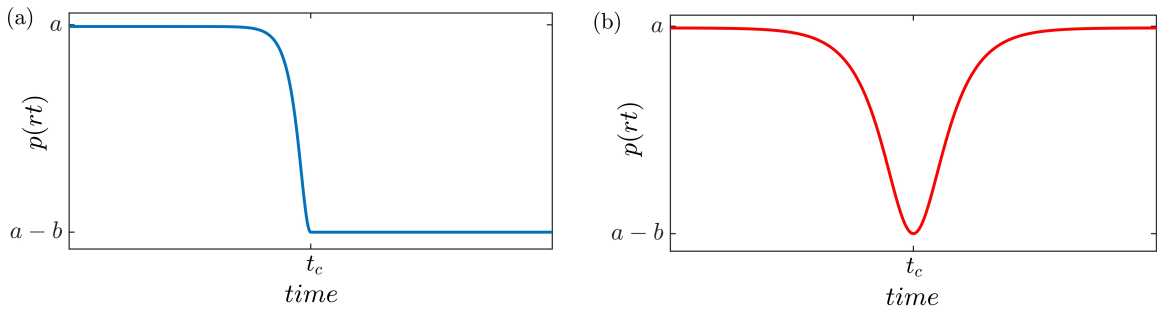


Figure 6. Examples of (a) monotone and (b) non-monotone time-dependent external inputs (7) and (8), respectively.

Furthermore, we refer to system (5) with a fixed in-time input parameter $p(rt) = p$,

$$\dot{X} = \frac{dX}{dt} = g(X, p), \quad (9)$$

as the *autonomous frozen system*. Note that when $p = p^-$ (or p^+), then the autonomous frozen system is referred to as the past (or future) limit system. Finally, we write

$$X(t, t_0, X_0),$$

to denote the solution of system (5) at time t started from X_0 at initial time t_0 . We also write

$$X(t, X_0; p),$$

to denote the solution of system (9) at time t started from initial condition X_0 at time $t = 0$ for a fixed-in-time input parameter p .

3 When to expect rate-induced phase-tipping

In this section, we discuss the concept of partial basin instability for limit cycles ([Alkhayuon et al 2021](#)) and show that it is a useful criterion for testing systems' susceptibility to RP-tipping. We start by characterising all points on a limit cycle by phases.

3.1 Phase of limit cycles

The solution $X(t, \gamma_0; p)$ to the autonomous frozen system (9) started from some $X_0 = \gamma_0 \in \mathbb{R}^2$ for a fixed p is periodic if there exists a constant $T > 0$ such that

$$X(t, \gamma_0; p) = X(t + T, \gamma_0; p),$$

for all $t \in \mathbb{R}$. The period of this solution is the minimum such T . It is convenient to parametrise points along a periodic solution by time t ,

$$\gamma_t := X(t, \gamma_0; p) \in \mathbb{R}^2 \quad \text{for any } t \in [0, T),$$

and define the corresponding cycle in the phase space in terms of γ_t ,

$$\Gamma(p) = \{\gamma_t : t \in [0, T)\} \subset \mathbb{R}^2.$$

Following Nakao (2016), we associate a *phase* φ_{γ_t} with each point γ_t along the cycle $\Gamma(p)$,

$$\varphi_{\gamma_t} := \frac{2\pi t}{T} \in [0, 2\pi). \quad (10)$$

Here, we choose γ_0 with phase $\varphi_{\gamma_0} = 0$ as follows: $\gamma_0 = (x_0, y_0) \in \Gamma_1(p)$, where $x_0 = \max\{x : (x, y) \in \Gamma_1(p)\}$, for the birhythmic van der Pol oscillator, and similarly, $\gamma_0 = (x_0, y_0) \in \Gamma_2(p)$, where $x_0 = \max\{x : (x, y) \in \Gamma_2(p)\}$, for the Decroly-Goldbeter glycolysis model. Fig. 7 shows the phases for $\Gamma_1(p)$ in the van der Pol oscillator and $\Gamma_2(p)$ in the Decroly-Goldbeter glycolysis model.

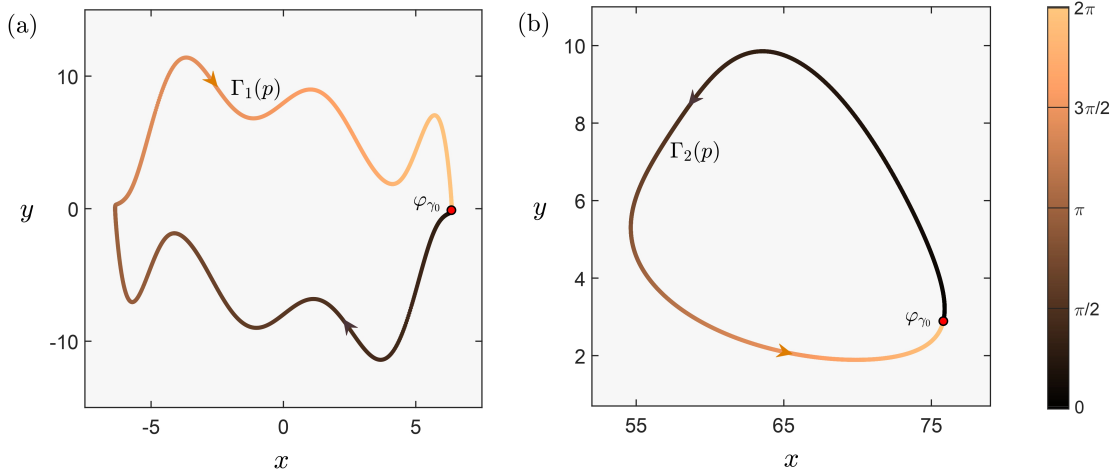


Figure 7. Heat map distribution of the phases $\varphi_{\gamma_t} \in [0, 2\pi)$ (defined in (10)) corresponding to the points γ_t on a limit cycle: For (a) $\Gamma_1(p)$ of the birhythmic van der Pol oscillator (2), where $p = \mu = 1.52$, and (b) $\Gamma_2(p)$ of the Decroly-Goldbeter glycolysis model (4), where $p = \sigma_i = 1.226$, starting at the initial phase φ_{γ_0} (red filled circle).

3.2 Partial basin instability of limit cycles

Partial basin instability for limit cycles (Alkhayuon et al 2021) is a simple geometric framework that uses global properties of the frozen autonomous system (9) to study RP-tipping. It compares the position of the base limit cycle at one point on a parameter path with the position of the basin of attraction of that limit cycle at other points on the parameter path.

Consider the base limit cycle $\Gamma(p)$ and its basin of attraction $B(\Gamma, p)$. Also, consider a parameter path Δ_p , on which $\Gamma(p)$ varies smoothly with p , meaning that $\Gamma(p)$ does not bifurcate along Δ_p . We say that $\Gamma(p)$ is *basin unstable* on Δ_p if there exist two points p_1 and p_2 in Δ_p such that $\Gamma(p_1)$

is not contained in the basin of attraction of $\Gamma(p_2)$,

$$\Gamma(p_1) \not\subset B(\Gamma, p_2). \quad (11)$$

Furthermore, $\Gamma(p)$ is *partially basin unstable* on Δ_p if, in addition to condition (11), for every two points $p_3, p_4 \in \Delta_p$, $\Gamma(p_3)$ has a nonempty intersection with $B(\Gamma, p_4)$. In other words, $\Gamma(p_3)$ never lies entirely outside of $B(\Gamma, p_4)$. If there exist \tilde{p}_3 and \tilde{p}_4 such that $\Gamma(\tilde{p}_3)$ has an empty intersection with $B(\Gamma, \tilde{p}_4)$, meaning that $\Gamma(\tilde{p}_3)$ lies entirely outside of $B(\Gamma, \tilde{p}_4)$, we say that $\Gamma(p)$ is *totally basin unstable* on Δ_p .[†]

In the autonomous frozen system (9), suppose that $\Gamma(p)$ is basin unstable on a parameter path Δ_p . For any given p_1 and p_2 in Δ_p , we will consider the set of all points on the limit cycle $\Gamma(p_1)$ that lie outside $B(\Gamma, p_2)$,

$$U(\Gamma, p_1, p_2) = \{\gamma_t : \gamma_t \in \Gamma(p_1) \text{ and } \gamma_t \notin B(\Gamma, p_2)\}.$$

We will be interested in the corresponding set of phases of $\Gamma(p_1)$, namely

$$\Phi_U(\Gamma, p_1, p_2) = \{\varphi_{\gamma_t} : \gamma_t \in U(\Gamma, p_1, p_2)\},$$

which we refer to as the (p_1, p_2) -basin unstable phases of $\Gamma(p)$, or basin unstable phases of $\Gamma(p)$ for short.

Furthermore, for a given parameter path Δ_p , we will consider the whole family of limit cycles $\Gamma(p)$ that vary smoothly with $p \in \Delta_p$,

$$G = \{\Gamma(p) : p \in \Delta_p\}.$$

For a fixed $p = p_1 \in \Delta_p$, we define the *parameter region of basin instability* of $\Gamma(p_1)$ as follows:

$$BI(\Gamma, p_1) := \{p_2 \in \Delta_p : \Gamma(p_1) \not\subset B(\Gamma, p_2)\}.$$

[†]Note that, there are indiscernible (or marginal) cases of basin instability that are not relevant to this work. For more details, see (Alkhayuon et al 2021, Sec. 4).

This is a set of all parameter values $p_2 \in \Delta_p$ such that $\Gamma(p_1)$ is not contained in the basin of attraction of $\Gamma(p_2)$.

3.3 Rate-induced phase-tipping from limit cycles

Consider the non-autonomous system (5) with sufficiently large t_c so that it resembles the past limit system for small $t \geq 0$. We choose initial conditions X_0 on the base limit cycle $\Gamma(p^-)$ of the past limit system[†] and, for simplicity, we write $X(t, 0, X_0) \rightarrow D$ as $t \rightarrow +\infty$ to denote $d[X(t, 0, X_0), D] \rightarrow 0$ as $t \rightarrow +\infty$, where

$$d[X, D] = \inf_{y \in D} \|X - y\|,$$

is the Hausdorff semi-distance between a point X and a compact set D .

We say that system (5) undergoes *irreversible* RP-tipping from $\Gamma(p^-)$ for the time-dependent external inputs (7) and (8) if there exists a critical rate $r = r_c$ in the following sense. For all $0 < r < r_c$ and every initial condition $X_0 \in \Gamma(p^-)$, the solution $X(t, 0, X_0)$ end-point tracks the base limit cycle, meaning that

$$X(t, 0, X_0) \rightarrow \Gamma(p^+) \text{ as } t \rightarrow +\infty.$$

However, for some $r > r_c$, there exist two points $X_{0,1}$ and $X_{0,2}$ on $\Gamma(p^-)$, such that the solution $X(t, 0, X_{0,1})$ started from $X_{0,1}$ end-point tracks the base limit cycle, whereas $X(t, 0, X_{0,2})$ started from $X_{0,2}$ end-point tracks some alternative attractor $A(p)$ other than $\Gamma(p)$. To be precise,

$$X(t, 0, X_{0,1}) \rightarrow \Gamma(p^+) \text{ as } t \rightarrow +\infty \quad \text{and} \quad X(t, 0, X_{0,2}) \rightarrow A(p^+) \text{ as } t \rightarrow +\infty.$$

Now, to each initial condition $X_{0,2} \in \Gamma(p^-)$ that gives RP-tipping from $\Gamma(p^-)$, we assign a (*tipping*) *phase* which is the phase of that point as specified in Sec. 3.1 and Fig. 7.

To make the connection between RP-tipping and partial basin instability, consider a partial basin unstable limit cycle $\Gamma(p)$ on a parameter path Δ_p . Partial basin instability implies there are

[†]Note that, $\Gamma(p^-)$ is not a limit cycle for system (5) and $p(0) \neq p^-$, but close enough for large t_c , see Eqs. (7) and (8).

two points $p^-, p^+ \in \Delta_p$, such that

$$\Gamma(p^-) \not\subset B(\Gamma, p^+) \quad \text{and} \quad \Gamma(p^-) \cap B(\Gamma, p^+) \neq \emptyset. \quad (12)$$

Now, consider a monotone external input $p(rt)$, given by Eq. (7), where $p(rt) \rightarrow p^\pm$ as $t \rightarrow \pm\infty$.

One can show that the system can exhibit RP-tipping, as follows:

1. For a slow external input (vanishing r), (Alkhayuon and Ashwin 2018, Theorem III.1) shows that the system will exhibit tracking, i.e., there will be $\tilde{r} > 0$ such that for every $X_0 \in \Gamma(p^-)$ and $0 < r < \tilde{r}$, we have

$$X(t, 0, X_0) \rightarrow \Gamma(p^+) \text{ as } t \rightarrow \infty.$$

2. For very fast external input ($r \rightarrow \infty$), condition (12) implies that there exist two points $X_{0,1}, X_{0,2} \in \Gamma(p^-)$ such that the trajectory started from $X_{0,1}$ end-point tracks $\Gamma(p)$ and the trajectory started from $X_{0,2}$ does not,

$$X(t, 0, X_{0,1}) \rightarrow \Gamma(p^+) \text{ as } t \rightarrow +\infty \quad \text{and} \quad X(t, 0, X_{0,2}) \not\rightarrow \Gamma(p^+) \text{ as } t \rightarrow +\infty.$$

3. By continuity, there must be at least one critical rate $r_c \geq \tilde{r}$ that gives RP-tipping.

In Section 4, we use the birhythmic van der Pol oscillator and Decroly-Goldbeter glycolysis model to illustrate RP-tipping.

4 Results

In this section, we analyse RP-tipping in both the birhythmic van der Pol and Decroly-Goldbeter glycolysis models. We start by identifying the regions of partial basin instability in the parameter space. Then, we illustrate RP-tipping in both models using tipping diagrams for the monotone and the non-monotone time-dependent external inputs. Unless stated otherwise, we will consider the stable limit cycle Γ_1 as the base state for the birhythmic van der Pol model, and Γ_2 as the base state for the Decroly-Goldbeter glycolysis model.

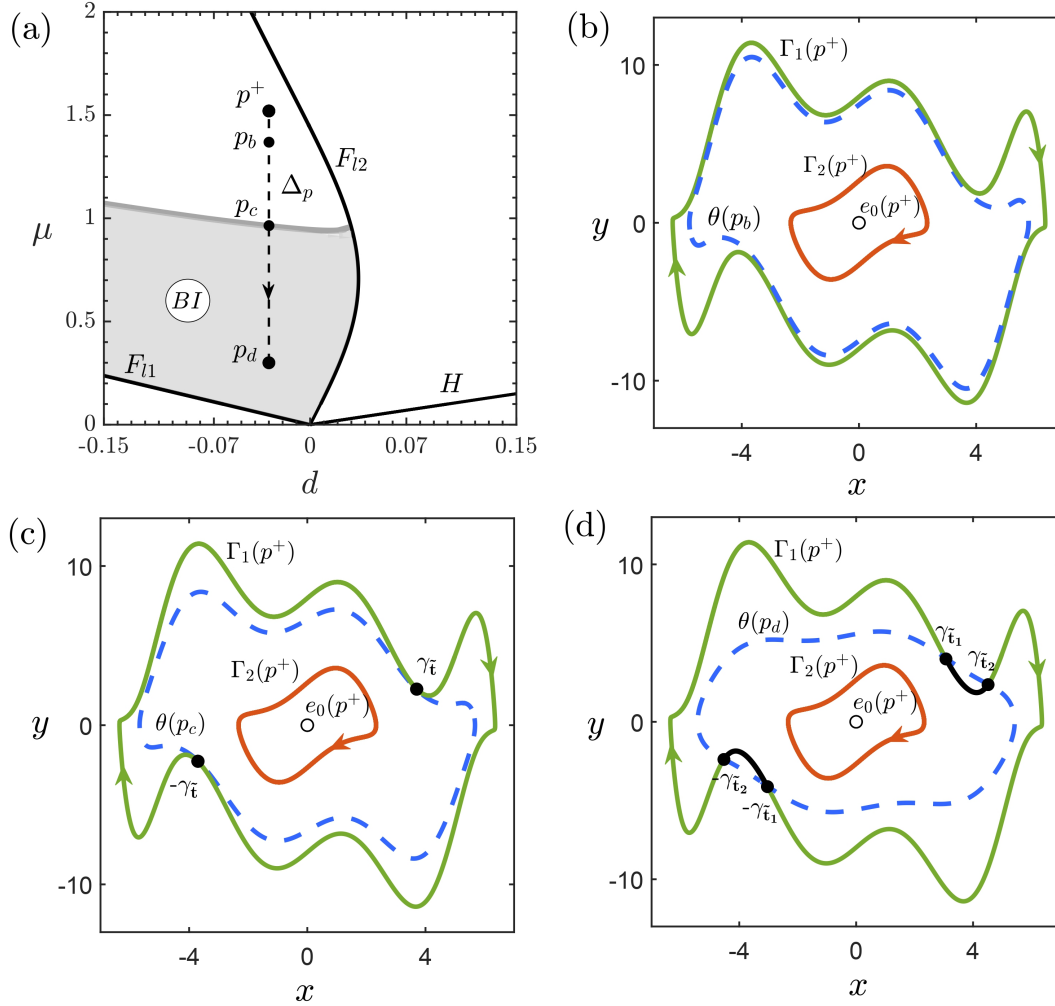


Figure 8. (a) Two-parameter bifurcation diagram (d vs μ) for the autonomous birhythmic van der Pol model (2), where the grey shaded area marks the region of partial basin instability (BI) of the base limit cycle $\Gamma_1(p^+)$. The vertical dashed line between p^+ and p_d represents a parameter path Δ_p , which is used to simulate other sub-figures. (b)-(d) Phase portraits with two stable limit cycles Γ_1 (green) and Γ_2 (orange), and an unstable equilibrium point e_0 for a fixed $p^+ = (d, \mu^+) = (-0.03, 1.52) \in \Delta_p$. In each phase portrait, the unstable limit cycle θ (blue dashed curve), which acts as a basin boundary between Γ_1 and Γ_2 , is plotted for different parameter settings: (b) with no basin instability for $p_b = (-0.03, 1.4) \in \Delta_p$, (c) with marginal basin instability at $\gamma_{\tilde{t}}$ (black dot) for $p_c = (-0.03, 1) \in \Delta_p$ where $\tilde{t} \approx 6.11$, and (d) with partial basin instability between $\gamma_{\tilde{t}_1}$ ($\tilde{t}_1 \approx 5.9$) and $\gamma_{\tilde{t}_2}$ ($\tilde{t}_2 \approx 6.51$) for $p_d = (-0.03, 0.3) \in \Delta_p$ (black curve on $\Gamma_1(p^+)$). The limit cycle $\Gamma_1(p^+)$ is also basin unstable at $-\gamma_{\tilde{t}}$ ($\tilde{t} \approx 2.61$) in (c), as well as between $-\gamma_{\tilde{t}_1}$ ($\tilde{t}_1 \approx 2.4$) and $-\gamma_{\tilde{t}_2}$ ($\tilde{t}_2 \approx 3.01$) in (d), owing to the inherent symmetry of the model (2).

4.1 Rate-induced Phase-tipping in the birhythmic van der Pol model

4.1.1 Partial basin instability in the birhythmic van der Pol model

Consider the two-parameter bifurcation diagram Fig. 2(a) for the birhythmic van der Pol model. We are interested in the birhythmic region-I, where RP-tipping can occur from the base limit cycle

Γ_1 . In Fig. 8(a), we augment the two-parameter bifurcation diagram Fig. 2(a) by adding the region of partial basin instability BI for the base limit cycle Γ_1 at a particular parameter point p^+ . In other words, the limit cycle $\Gamma_1(p^+)$ is partial basin unstable on any parameter path that crosses into the grey region BI . To illustrate this effect, we consider the parameter path Δ_p , which does not cross any bifurcation curve, and consider three points along this path: p_b in the white region, p_c on the boundary, and p_d inside the grey region. Figs. 8(b)-8(d) show the stable limit cycles $\Gamma_{1,2}(p^+)$ in comparison with the unstable limit cycle $\theta(p)$, where $p = p_b, p_c$, and p_d , respectively. Note that $\theta(p)$ represents the boundary of the basin of attraction of the base limit cycle. One can see that in Fig. 8(b), the base limit cycle $\Gamma_1(p^+)$ does not intersect the basin boundary $\theta(p_b)$, indicating no basin instability. However, in Fig. 8(d), there is a set of phases that are basin unstable (black) due to $\theta(p_d)$. The base limit cycle tangentially intersects the basin boundary $\theta(p_c)$ (see Fig. 8(c)) if the parameter path ends at point p_c ; in such a case, $\Gamma_1(p^+)$ is marginally basin unstable (Alkhayoun et al 2021). From Section 3.3, we expect RP-tipping from $\Gamma_1(p^+)$ if the external input varies on the parameter path Δ_p .

Furthermore, we point out that due to the symmetry of the model, the unstable limit cycle $\theta(p_c)$, in Fig. 8(c) tangentially intersects $\Gamma_1(p^+)$ at two points $\gamma_{\tilde{t}}$ and $-\gamma_{\tilde{t}}$, resulting in the possibility of basin instability at two locations and expanded further to give basin unstable phases between $\gamma_{\tilde{t}_1}$ ($-\gamma_{\tilde{t}_1}$) and $\gamma_{\tilde{t}_2}$ ($-\gamma_{\tilde{t}_2}$) in Fig. 8(d).

Considering the basin instability of $\Gamma_1(p)$ and the possibility of RP-tipping, one is tempted to look at the basin instability of the two stable limit cycles $\Gamma_1(p)$ and $\Gamma_2(p)$ for different points on the same parameter path. In Fig. 9, we consider two points \bar{p}^- and \bar{p}^+ from a parameter path $\Delta_{\bar{p}}$ that is longer than previously considered Δ_p . We then compute the basin instability region of $\Gamma_2(\bar{p}^+)$, denoted by BI_1 in Fig. 9(a), as well as, the basin instability region of $\Gamma_1(\bar{p}^-)$, denoted by BI_2 in Fig. 9(b). Although the BI_1 region is considerably small, having both basin instabilities on the same parameter path opens the possibility of alternating series of RP-tipping from $\Gamma_2(\bar{p})$ to $\Gamma_1(\bar{p})$ and vice versa if the external input varies non-monotonically on $\Delta_{\bar{p}}$. We illustrate this behaviour in Section 4.1.3.

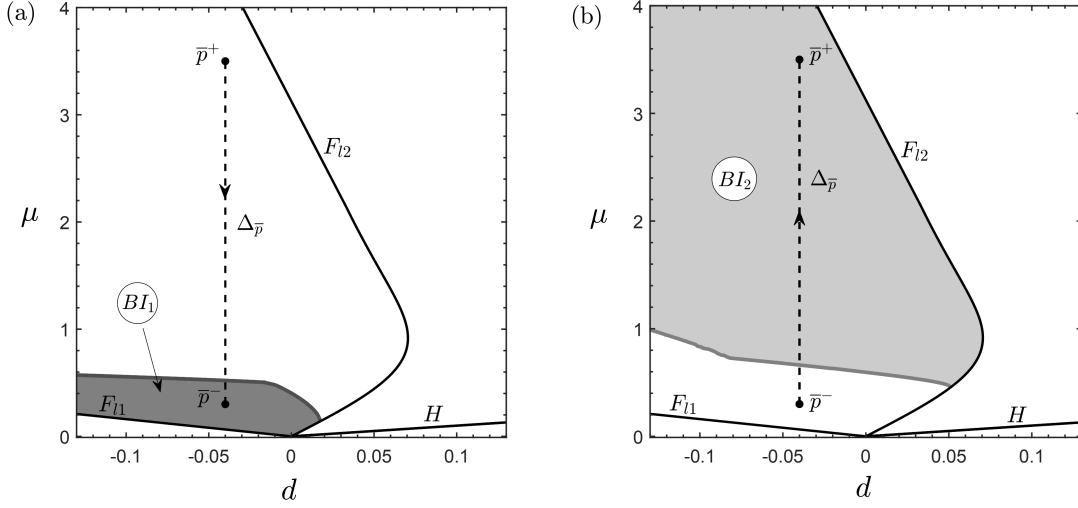


Figure 9. Two-parameter bifurcation diagrams of the birhythmic van der Pol model (2) with the variation in the parameters d vs. μ . In (a), the dark grey shaded area denotes the region of partial basin instability (BI_1) corresponding to the base state $\Gamma_2(\bar{p}^+)$ with the parameter path $\Delta_{\bar{p}}$ varied along the direction from $\bar{p}^+ = (-0.04, 3.5)$ to $\bar{p}^- = (-0.04, 0.3)$, whereas, the light grey region in (b) denotes the region of partial basin instability (BI_2) correspond to the base state $\Gamma_1(\bar{p}^-)$ along with the parameter path $\Delta_{\bar{p}}$ varied from \bar{p}^- to \bar{p}^+ . Grey curves separating the grey and white regions in both figures represent the marginal basin unstable curves. The other parameter values are $\alpha = 0.0938$ and $\beta = 0.00194$.

4.1.2 Rate-induced Phase-tipping diagrams for the van der Pol model

In this section, we use tipping diagrams to analyse RP-tipping in the birhythmic van der Pol model for both monotone and non-monotone external inputs. Throughout this section, the external input varies along the parameter path Δ_p , presented in Fig. 8(a). In other words, we fix the parameter $d = -0.03$ and vary the input parameter μ following Eqs. (7) and (8) with $a = \mu^+$ and $b = \mu^+ - \mu^-$, we recall that b is the magnitude of the external input. Rate-induced diagrams (or tipping diagrams for short) are two-parameter representations of tipping and tracking behaviour, i.e., the rate of change r versus the magnitude of an external input b (O’Keeffe and Wiczeorek 2020).

Fig. 10(a) presents a tipping diagram for model (2), with a monotone input $\mu(rt)$ (7) that transitions from μ^+ to μ^- along the path Δ_p . The figure is produced by solving the system for one initial condition $X_0 \approx (4, 1.89)$ on the base limit cycle $\Gamma_1(\mu^+)$ at time $t = 0$. The peak of the shift is fixed at time $t = t_c$, which is 4 times the period (T) of the base limit cycle. The green region represents r and b values where the trajectory tracks the base limit cycle $\Gamma_1(\mu^-)$, whereas the red region represents r and b values where the trajectory tips to the alternative limit cycle $\Gamma_2(\mu^-)$. The red curve, which forms the boundary between these regions, indicates the critical rates r_c for

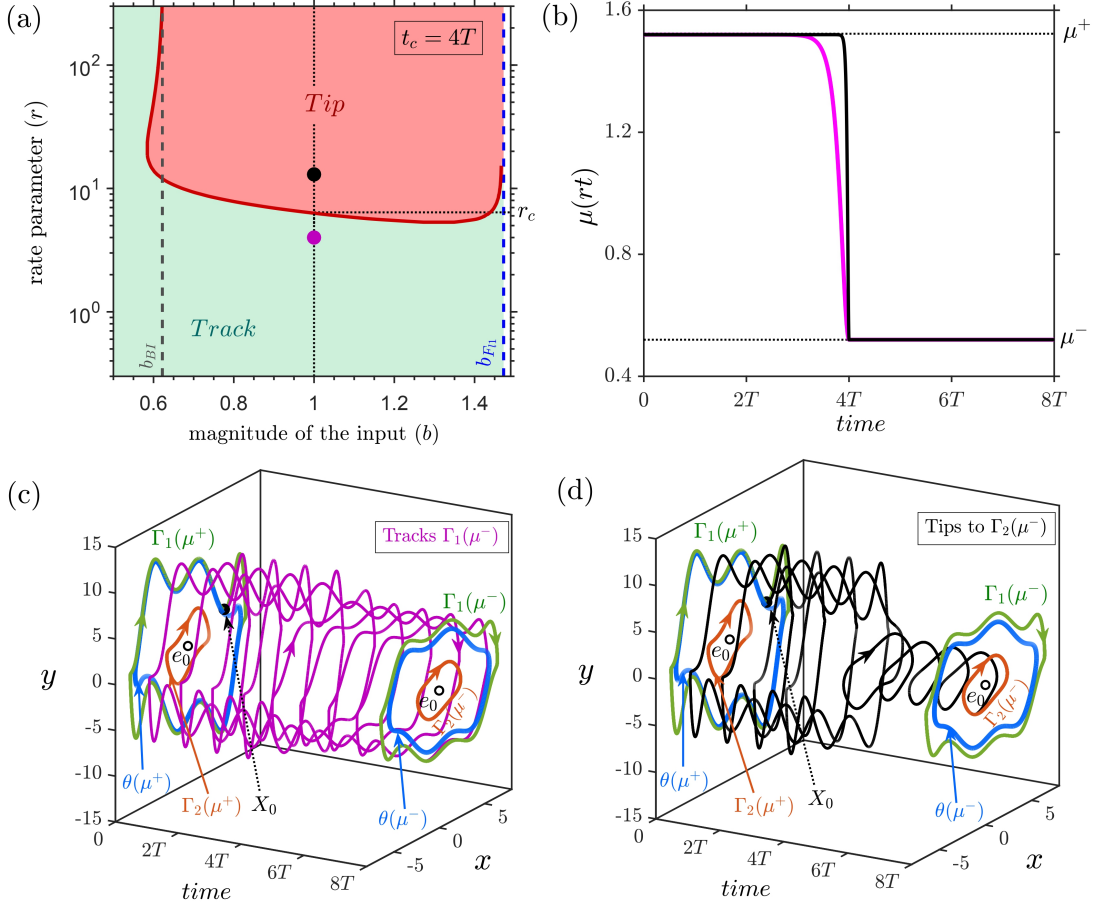


Figure 10. (a) Half-bounded tipping diagram for the birhythmic van der Pol oscillator (2) with variations in the parameters of monotone shift $\mu(rt)$ (7): magnitude (b) vs. rate (r) for the fixed value of $t_c = 4T$, where $T = 6.9979$ is period of the limit cycle $\Gamma_1(\mu^+)$. The red region (Tip) signifies the parameter space that results in RP-tipping, while the green region (Track) represents tracking. The red curve, which forms the boundary between the tipping and tracking regions, provides a critical rate r_c of the monotone shift for a fixed magnitude b . The blue and grey vertical dashed lines indicate the fold point $b_{F_{11}}$ and basin unstable phase b_{BI} , respectively. (b) The evolution of the monotone parameter shifts $\mu(rt)$ between μ^+ and μ^- with respect to time for fixed b and different values of the rate r (same as the coordinate and colour scheme of the filled circles in (a)). (c)-(d) Phase portraits with trajectories originating from the initial point $X_0 = (4, 1.89)$ on $\Gamma_1(\mu^+)$ for the fixed magnitude $b = 1$ and different rates $r_1 = 4$ (magenta) and $r_2 = 13$ (black) of the monotone shift as pointed in (a). The trajectory tracks $\Gamma_1(\mu^-)$ for the rate r_1 ; whereas, for r_2 it tips to the limit cycle $\Gamma_2(\mu^-)$ (see the electronic supplementary material).

each value of b . Here, the tipping region is half-bounded. In the sense that, for each large enough magnitude b there is a critical rate r_c below which there is no tipping. We point out that when r is large, the boundary of the tipping region is asymptotic to $b_{BI} = 0.622$ (vertical grey dashed line), which corresponds to the basin unstable phase of an initial condition X_0 . On the other hand, we do not allow the external input to exceed the fold of limit cycles $b_{F_{11}} = 1.4725$ (vertical blue dashed line). To illustrate the tipping and tracking behaviour, we chose two points on the diagram

that corresponds to the rates $r_1 = 4$ and $r_2 = 13$ (the magenta and black dots) for a fixed $b = 1$. Fig. 10(b) shows the external forcing in time concerning rates r_1 and r_2 , and Fig. 10(c) shows the magenta trajectory with the rate r_1 is tracking $\Gamma_1(\mu^-)$, while Fig. 10(d) shows the black trajectory with r_2 is tipping to the alternative limit cycle $\Gamma_2(\mu^-)$.

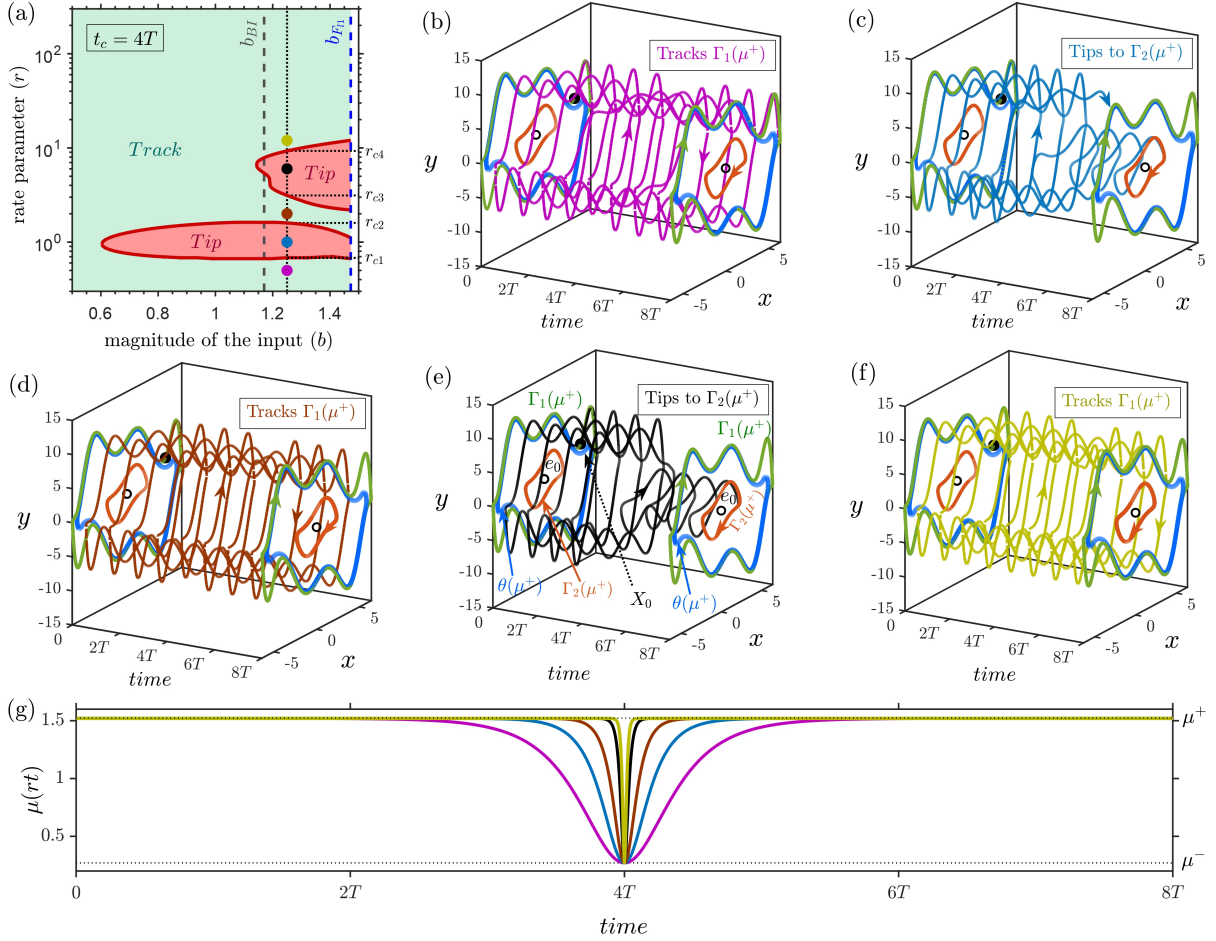


Figure 11. (a) Bounded tipping diagram for the birhythmic van der Pol oscillator (2) with variations in the parameters of non-monotone shift $\mu(rt)$ (8): magnitude (b) vs. rate (r) for the fixed value of $t_c = 4T$, where T is period of the limit cycle $\Gamma_1(\mu^+)$. The red region (Tip) signifies the parameter values that result in RP-tipping from $\Gamma_1(\mu^+)$ to $\Gamma_2(\mu^+)$, while the green region (Track) represents tracking to $\Gamma_1(\mu^+)$. The boundary curves (red) that separate the tipping and tracking regions provide critical rates r_c of the non-monotone shift for a fixed magnitude b . The critical rates r_{c1}, r_{c2}, r_{c3} and r_{c4} correspond to the magnitude $b = 1.25$. The blue and grey vertical dashed lines indicate the fold point $b_{FI} = 1.4725$ and basin unstable phase $b_{FI} = 1.17$ corresponding to the initial condition X_0 in other sub-figures, respectively. (b)-(f) Phase portraits with trajectories originating from the initial point $X_0 = (4.503, 2.33)$ on $\Gamma_1(\mu^+)$ for the fixed magnitude $b = 1.25$ and different rates $r_1 = 0.5$ (magenta), $r_2 = 1$ (blue), $r_3 = 2$ (brown), $r_4 = 6$ (black), and $r_5 = 12$ (yellow-green) as pointed in (a). For the rates r_1, r_3 and r_5 , it is observed that trajectories track the limit cycle $\Gamma_1(\mu^+)$; whereas for the rates r_2 and r_4 , trajectories tip to the alternative limit cycle $\Gamma_2(\mu^+)$ (see the electronic supplementary material). (g) The evolution of non-monotone parameter shifts $\mu(rt)$ with respect to time for fixed b and different values of the rate r (same as the coordinate and colour scheme of the filled circles in (a)).

Next, we consider model (2) with a non-monotone external input from μ^+ to μ^- and then back

to μ^+ following Eqn. (8), with the peak of the external input take place at time $t = t_c$, which is 4 times the period (T). Fig. 11(a) presents a tipping diagram with tipping regions bounded by tipping curves (red). In (O’Keeffe and Wieczorek 2020), the authors refer to such bounded tipping regions as tipping tongues. Similar to the monotone case, we do not allow the magnitude of the external input b to exceed the fold of limit cycles $b_{F_{l_1}} = 1.4725$ (blue dashed line).

The tipping diagram delineates two distinct regions, red (*Tip*) and green (*Track*), representing RP-tipping and tracking. The vertical grey dashed line indicates the basin unstable phase $b_{BI} = 1.17$ corresponds to the initial condition $X_0 \approx (4.503, 2.33)$ on the base limit cycle $\Gamma_1(\mu^+)$. The three-dimensional phase portraits in Figs. 11(b)-11(f) illustrate these tipping and tracking behaviours starting from X_0 . For a fixed magnitude $b = 1.25$, five distinct rates are chosen (see Fig. 11 caption for rate values), each represented by a different colour in Fig. 11(a). Among these, the rates r_1 , r_3 , and r_5 are located in tracking regions, while r_2 and r_4 are in tipping regions. As chosen rates in different regions, the trajectories in Figs. 11(b), 11(d), and 11(f) track the same stable limit cycle $\Gamma_1(\mu^+)$, while the trajectories in Figs. 11(c), and 11(e) tip to an alternative stable limit cycle $\Gamma_2(\mu^+)$. Fig. 11(g) illustrates the non-monotone shifts corresponding to distinct rates.

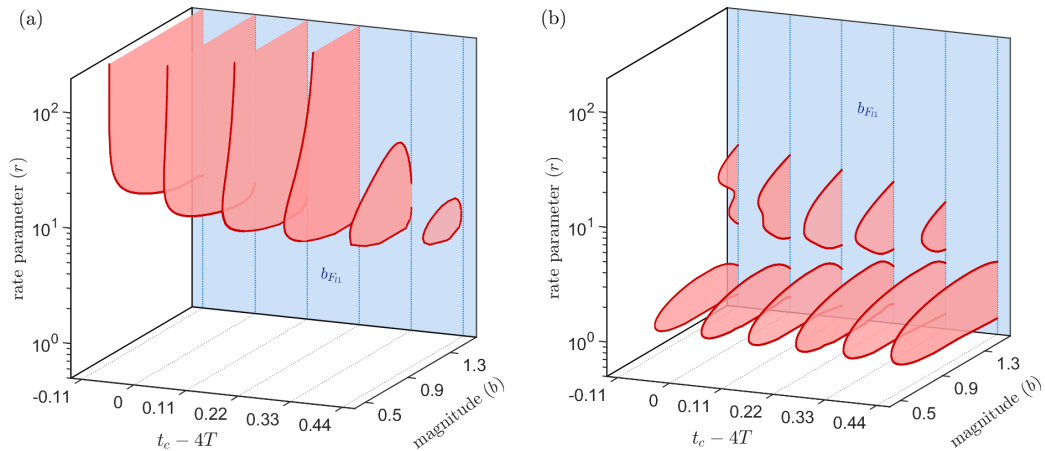


Figure 12. Three-dimensional tipping diagrams of the birhythmic van der Pol model (2) with variations in the parameters (t_c vs. b vs. r) for (a) monotone input (7) and (b) non-monotone input (8), for different values of t_c starting from $4T - 0.11$ to $4T + 0.44$ with an increment of 0.11. The blue plane denotes the fold point $b_{F_{l_1}}$.

For a fixed value of $t_c = 4T$, which aligns with the phase of the initial condition X_0 of the trajectory, and for one trajectory, tipping diagrams reveal distinct characteristics of the tipping region: half-bounded for monotone input and fully bounded with two sub-regions for non-monotone

input. This observation prompts an investigation into the relationship between the phases of the limit cycle and the tipping diagrams associated with both inputs described by (7) and (8). For a fixed initial condition X_0 , one expects these tipping diagrams to vary while changing t_c . Also, here, we recall that our definition for the tipping phase is dependent on t_c . We find that changing the t_c value alters the shape of rate-induced phase tipping diagrams, as illustrated in Fig. 12(a) for the monotone input. A gradual change in the value of t_c by increments of 0.11 shows that the half-bounded tipping regions become fully bounded. Also, in the case of non-monotone input (8), for variation in t_c values, the impact of phase on the tipping diagrams can be seen in Fig. 12(b). It is observed that previously separated tipping regions merge, forming a single tipping region as t_c varies.

4.1.3 Series of rate-induced phase-tipping between limit cycles

In Section 4.1.1, we pointed out that there is a possibility of a series of alternating tipping between $\Gamma_1(p)$ and $\Gamma_2(p)$ in the van der Pol model. In this section, we illustrate this behaviour using a new non-monotone external input in the form of impulse (Hasan et al 2023):

$$\mu(rt) = \mu^- + b \left[\frac{\tanh(r(t - t_{c1})) - \tanh(r(t - t_{c2}))}{2} \right]. \quad (13)$$

In this non-monotone input, $\mu(rt) \approx \mu^+ = \mu^- + b$ for a time interval of length $t_{c2} - t_{c1}$, which allows the system to settle into the new regime before shifting it back to $\mu(rt) \approx \mu^-$, see Fig. 13(e). In Fig. 13, we vary the input parameter along the parameter path $\Delta_{\bar{p}}$ shown in Fig. 9, where we fix the parameter $d = -0.04$ and vary the parameter $\mu(rt)$ between $\mu^- = 0.3$ and $\mu^+ = 3.5$ according to (13). We also fix the rate parameter $r = 27$ and illustrate possible tipping and tracking combinations. The non-autonomous trajectories are depicted in solid black; green and orange trajectories represent base limit cycles Γ_1 and Γ_2 , respectively, for fixed in-time input μ . The 4 trajectories in Figs. 13(a)-13(d) start at different initial conditions X_a, X_b, X_c and X_d all on the limit cycle $\Gamma_1(\mu^-)$, at time $t = 0$. In Fig. 13(a), the trajectory tracks Γ_1 all the way to the end. In Fig. 13(b), the trajectory tracks initially but then tips to $\Gamma_2(\mu^-)$ after the second switch. In Fig. 13(c), the trajectory tips at the first switch to $\Gamma_2(\mu^+)$ and keeps tracking Γ_2 afterwards. Finally, in Fig. 13(d), the trajectory tips twice, from $\Gamma_1(\mu^-)$ to $\Gamma_2(\mu^+)$ at the first switch and back

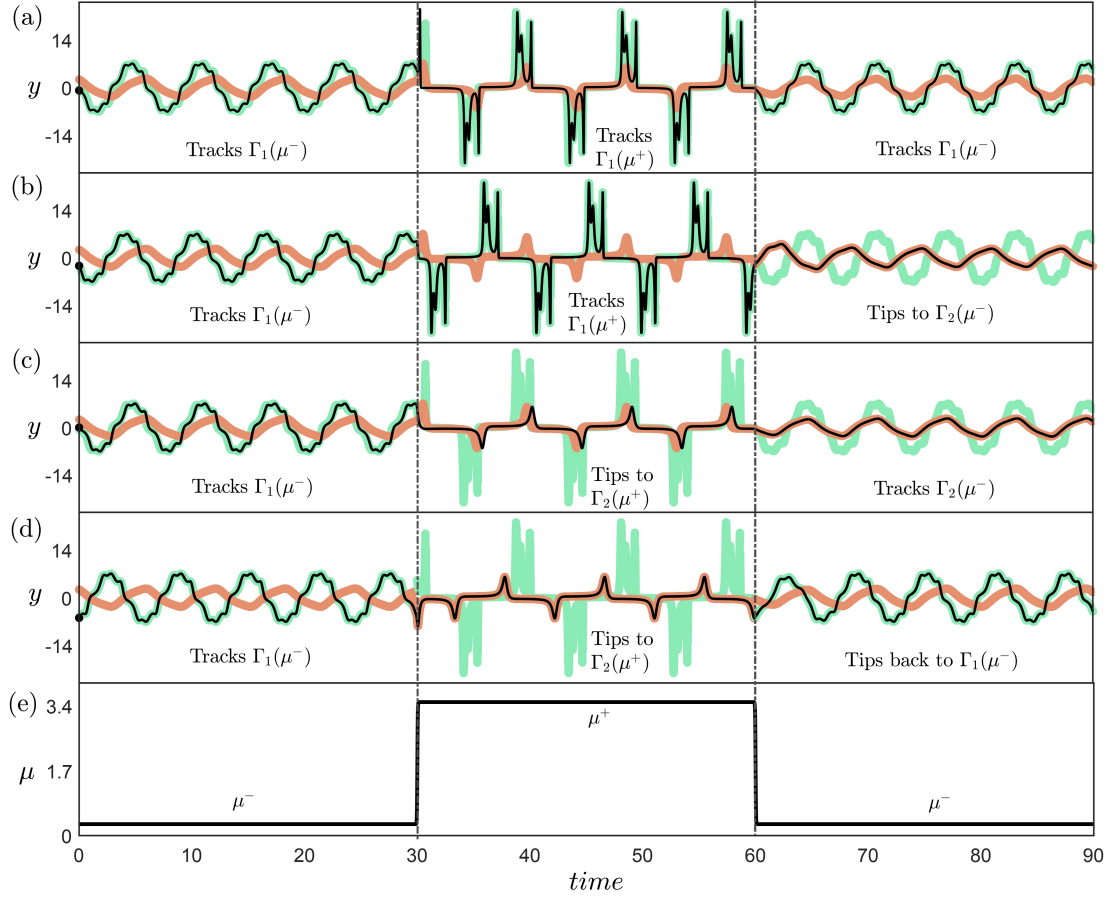


Figure 13. (a-d) Time series showing a series of tracking-tipping trajectories (black) of the birhythmic van der Pol model (2) for the non-monotone input (13) at a single rate value $r = 27$ and different initial conditions on $\Gamma_1(\mu^-)$. These are shown along with the base stable limit cycles Γ_1 (green) and Γ_2 (orange) of the corresponding autonomous frozen system (2). In (a), the trajectory always tracks the base limit cycle Γ_1 with an initial condition $X_a = (6.45, -0.858)$. In (b), the trajectory tips to an alternative base state $\Gamma_2(\mu^-)$ at $t_{c2} = 60$ from $X_b = (5.77, -2.372)$. In (c), the trajectory from $X_c = (6.5726, -0.0013)$ tips to the alternative state $\Gamma_2(\mu^+)$ at $t_{c1} = 30$ and continues to track the same base state $\Gamma_2(\mu^-)$ despite of a change in the value of μ . In (d), the trajectory from $X_d = (-2.7483, -5.9173)$ tips to $\Gamma_2(\mu^+)$ at $t_{c1} = 30$, tracks it until $t_{c2} = 60$, then tips back to $\Gamma_1(\mu^-)$. (e) The non-monotone time-dependent external input $\mu(rt)$ (13) in the form of an impulse.

to $\Gamma_1(\mu^-)$ at the second switch.

4.2 Rate-induced phase-tipping in the Decroly-Goldbeter glycolysis model

4.2.1 Partial basin instability in the Decroly-Goldbeter glycolysis model

Here, we study partial basin instability in the model (4) of birhythmic glycolytic oscillations. Consider the two-parameter bifurcation diagram in Fig. 4(a). We are interested in the birhythmic region-I, where RP-tipping can occur from the base limit cycle. In Fig. 14(a), we augment the

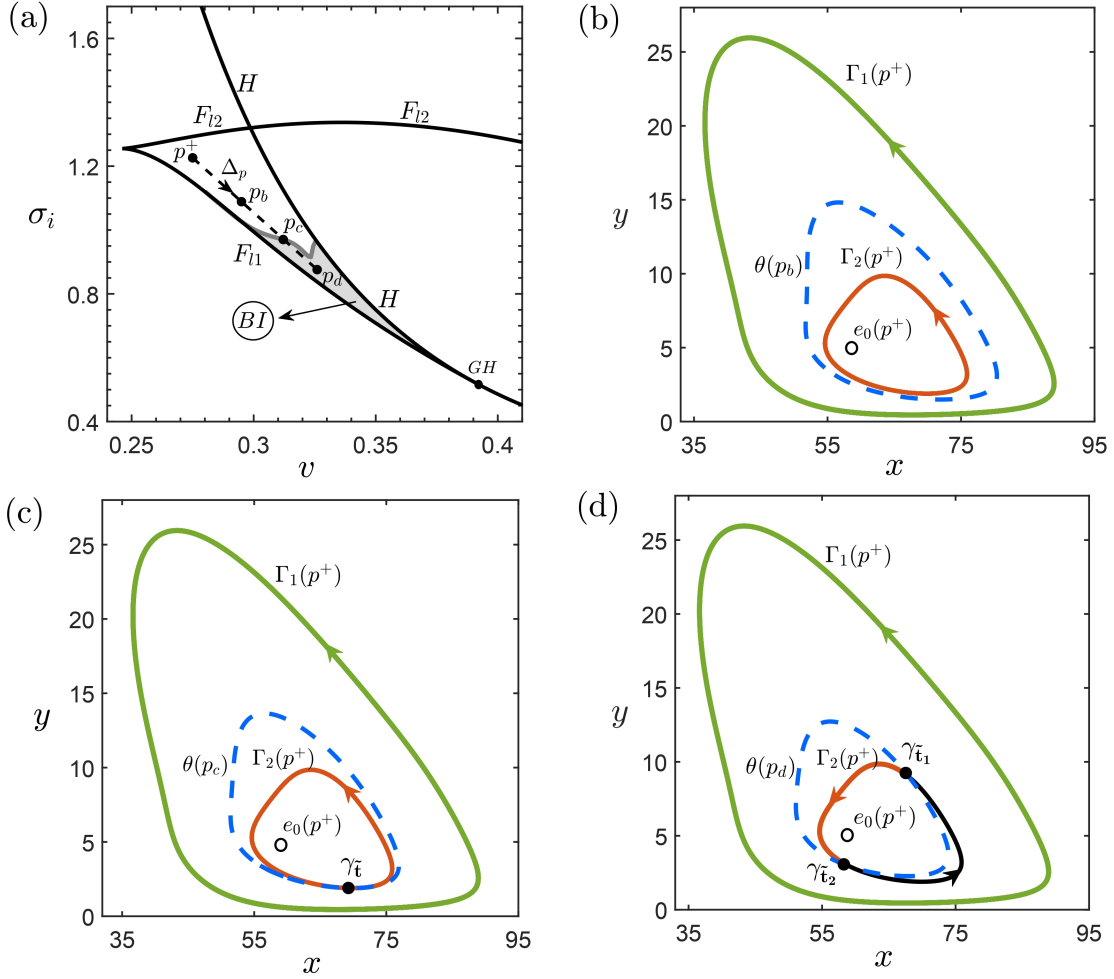


Figure 14. (a) Two-parameter bifurcation diagram (v vs σ_i) for the autonomous glycolysis model (4), where the grey shaded area marks the region of partial basin instability (BI) corresponding to the base limit cycle $\Gamma_2(p^+)$. (b)-(d) Phase portraits with two stable limit cycles Γ_1 (green) and Γ_2 (orange), and an unstable equilibrium point e_0 for a fixed $p^+ = (v^+, \sigma_i^+) = (0.275, 1.226)$. In each phase portrait, the unstable limit cycle θ (blue dashed curve), which acts as a basin boundary between Γ_1 and Γ_2 , is plotted for different parameter settings along the parameter path Δ_p : (b) with no basin instability for $p_b = (0.295, 1.0887)$, (c) with marginal basin instability at $\gamma_{\tilde{t}}$ (black dot) for $p_c = (0.312, 0.9702)$ where $\tilde{t} \approx 249.8$, and (d) with partial basin instability between $\gamma_{\tilde{t}_1}$ ($\tilde{t}_1 \approx 32.17$) and $\gamma_{\tilde{t}_2}$ ($\tilde{t}_2 \approx 179.31$) for $p_d = (0.326, 0.876)$ (black curve on $\Gamma_2(p^+)$).

two-parameter bifurcation diagram by adding the region of partial basin instability BI for the base limit cycle at a particular parameter point p^+ . In contrast to the van der Pol model (2), in this model, the limit cycle $\Gamma_2(p^+)$ is basin unstable on any parameter path that crosses into the grey region BI . To illustrate this effect, consider the parameter path Δ_p , which does not cross any bifurcation curve, and consider three points along this path: p_b in the white region, p_c on the boundary, and p_d in the grey region. This path is strategically chosen along the diagonal connecting points p^+ and p_d to induce basin instability. The corresponding Figs. 14(b), 14(c), and 14(d) show

the stable limit cycles $\Gamma_{1,2}(p^+)$ in comparison with the unstable limit cycle $\theta(p)$, where $p = p_b, p_c$, and p_d . $\theta(p)$ represents the boundary of the basin of attraction of the base limit cycle. One can see that in Fig. 14(b), the base limit cycle does not intersect the basin boundary and, hence, has no basin instability. However, in Fig. 14(d), there is a set of basin unstable phases (black). The base limit cycle tangentially intersects the basin boundary if the parameter path ends at point p_c (see Fig. 14(c)); in such a case, the base limit cycle is marginally basin unstable (Alkhayuon et al 2021). Again, from Section 3.3, we expect RP-tipping from $\Gamma_2(p^+)$ if the external input varies on the parameter path Δ_p .

4.2.2 Rate-induced Phase-tipping diagrams of the Decroly-Goldbeter glycolysis model

Similar to the van der Pol model, we investigate RP-tipping in the model (4) using the tipping diagrams for both monotone and non-monotone external inputs. The external input varies along the parameter path Δ_p , as shown in Fig. 14(a). Specifically, we vary the parameter σ_i between σ_i^+ and σ_i^- along the diagonal parameter path $v \approx (-\sigma_i + 3.11)/6.86$ following Eqs. (7) and (8), with $a = \sigma_i^+$ and $b = \sigma_i^+ - \sigma_i^-$, where b represents the magnitude of the external input.

First, we examine the model (4) with a monotone shift (7) of the external input $\sigma_i(rt)$ where the parameter transitions from σ_i^+ to σ_i^- . Fig. 15(a) displays a tipping region for a fixed value of t_c , which is half-bounded (O’Keeffe and Wieczorek 2020). Specifically, as the rate r increases, the boundary of the tipping region asymptotically approaches $b_{BI} = 0.2762$ (grey dashed line), corresponding to the basin instability of the initial condition $X_0 \approx (75.706, 2.76)$. The peak of the shift is set at $t = t_c$, which is four times the period (T) of the limit cycle. The tipping diagram includes a fold point $b_{F_{I1}} = 0.526$ (blue dashed line) beyond which the system exhibits B-tipping. The green region indicates values of r and b where the trajectory follows the base limit cycle $\Gamma_2(\sigma_i^-)$, whereas the red region indicates values of r and b where the trajectory tips to an alternative limit cycle $\Gamma_1(\sigma_i^-)$. The boundary curve (red) delineating these regions denotes the critical rates r_c for a fixed value of b . To illustrate the tipping and tracking behaviour, two points on the diagram for rates r_1 and r_2 (the magenta and black dots) were selected for the fixed $b = 0.35$. Fig. 15(b) shows the external forcing corresponding to both rates r_1 and r_2 . Figs. 15(c) and 15(d) demonstrate that the magenta trajectory with rate r_1 tracks the base limit cycle $\Gamma_2(\sigma_i^-)$, while the black trajectory

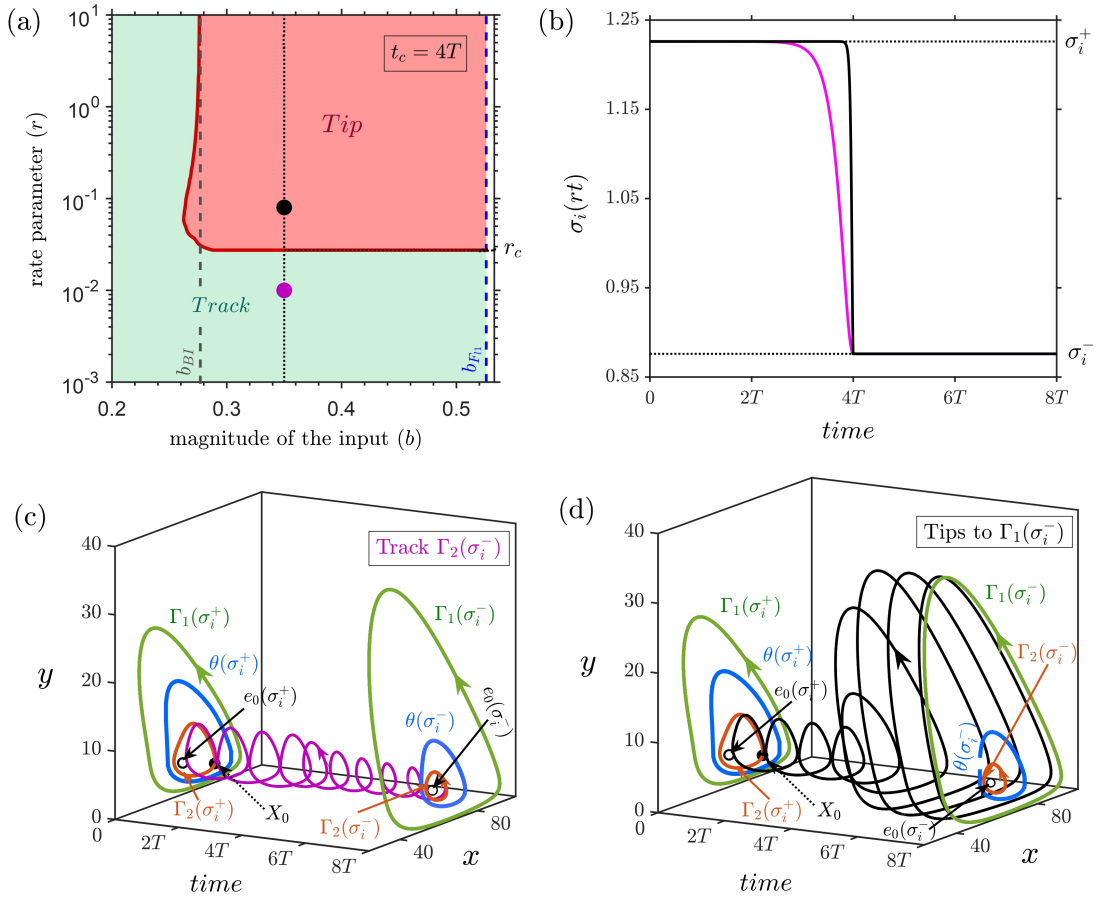


Figure 15. (a) Half-bounded tipping diagram for the Decroly-Goldbeter glycolysis model (4) with variations in the parameters of monotone shift $\sigma_i(rt)$ (7): magnitude (b) vs. rate (r) for the fixed value of $t_c = 4T$, where $T = 308.266$ is the period of $\Gamma_2(\sigma_i^+)$. The red region (Tip) signifies the parameter values that result in RP-tipping, while the green region (Track) represents tracking. The horizontal black dotted line corresponds to the critical rate r_c on the boundary curve for a fixed magnitude b . The blue and grey dashed lines indicate the fold point $b_{F_{l1}} = 0.526$ and basin unstable phase $b_{BI} = 0.2762$, respectively. (b) The evolution of monotone parameter shifts $\sigma_i(rt)$ between σ_i^+ and σ_i^- with respect to time, for fixed b and different values of the rate r (same as the coordinate and colour scheme of the filled circles in (a)). (c)-(e) Phase portraits with trajectories originating from the initial point $X_0 = (75.71, 2.76)$ on $\Gamma_2(\sigma_i^+)$, for the fixed magnitude $b = 0.35$ and different rates $r_1 = 0.01$ (magenta) and $r_2 = 0.08$ (black) of the monotone shift as pointed in (a). The trajectory tracks the limit cycle $\Gamma_2(\sigma_i^+)$ for the rate r_1 ; whereas for the rate r_2 , the trajectory tips to the limit cycle $\Gamma_1(\sigma_i^-)$ (see the electronic supplementary material).

with rate r_2 tips to the alternative limit cycle $\Gamma_1(\sigma_i^-)$, respectively.

Next, we examine model (4) with a non-monotone shift (8) of the external input $\sigma_i(rt)$ where the parameter transitions from σ_i^+ to σ_i^- and then returns to σ_i^+ . Fig. 16(a) displays a tipping tongue for a fixed value of t_c . This figure is generated by solving the system from an initial condition $X_0 \approx (68.91, 8.614)$ on the base limit cycle $\Gamma_2(\sigma_i^+)$ at time $t = 0$. The basin unstable point $b_{BI} = 0.341$ corresponds to X_0 and is marked with a vertical grey dashed line. The fold point $b_{F_{l1}} = 0.526$ is indicated by a blue dashed line, beyond which B-tipping occurs. The green region

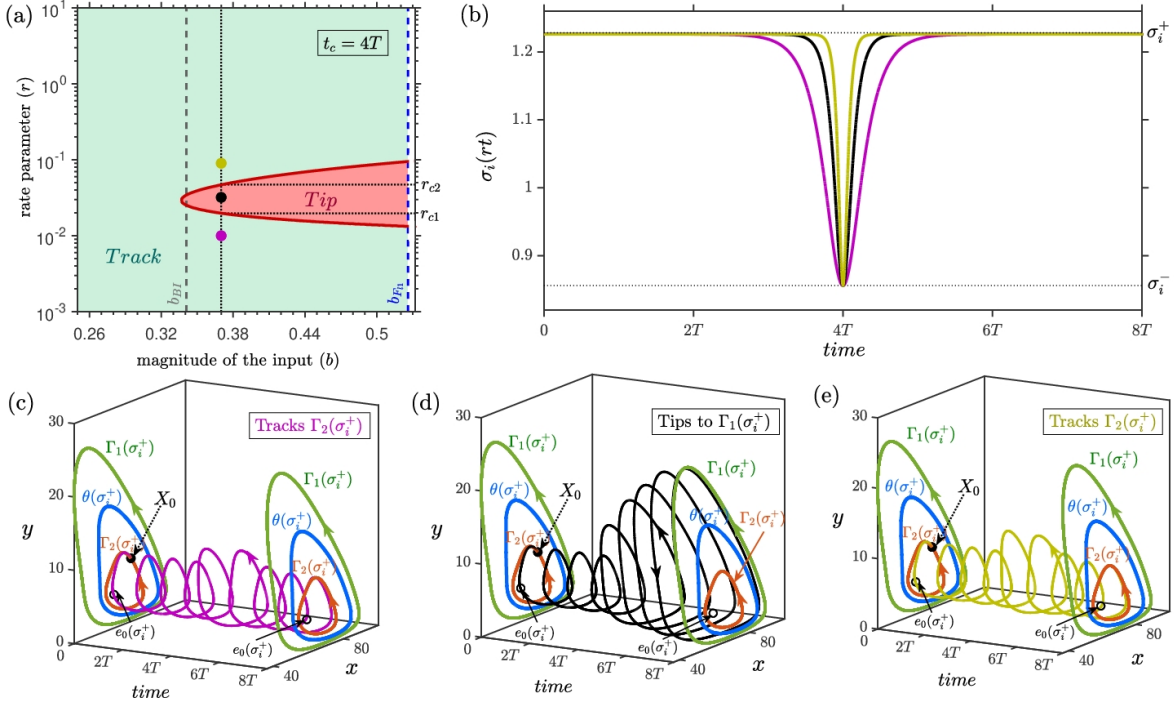


Figure 16. (a) Bounded tipping diagram for the Decroly-Goldbeter glycolysis model (4) with variations in the parameters of non-monotone shift $\sigma_i(rt)$ (8): magnitude (b) vs. rate (r) for the fixed value of $t_c = 4T$, where T is the period of the base limit cycle $\Gamma_2(\sigma_i^+)$. The red and green regions denote RP-tipping and tracking, separated by a boundary curve (red). r_{c1} and r_{c2} represent critical rates correspond to the magnitude $b = 0.37$. The blue and grey dashed lines indicate the fold point $b_{FI} = 0.526$ and basin unstable phase $b_{BI} = 0.341$, respectively. (b) The evolution of non-monotone parameter shifts $\sigma_i(rt)$ with respect to time for fixed b and different values of the rate r (same as the coordinate and colour scheme of the filled circles in (a)). (c)-(e) Phase portraits with trajectories originating from the initial point $X_0 = (68.91, 8.61)$ on $\Gamma_2(\sigma_i^+)$, for the fixed magnitude $b = 0.37$ and different rates $r_1 = 0.01$ (magenta), $r_2 = 0.032$ (black), and $r_3 = 0.09$ (grey) of the non-monotone shift as pointed in (a). For the rates r_1 and r_3 , it is observed that the trajectory tracks the limit cycle $\Gamma_2(\sigma_i^+)$; whereas for the rate r_2 , the trajectory tips to the limit cycle $\Gamma_1(\sigma_i^+)$ (see the electronic supplementary material).

indicates values of r and b where the trajectory follows the base limit cycle $\Gamma_2(\sigma_i^+)$, whereas the red region indicates values of r and b where the trajectory tips to an alternative limit cycle $\Gamma_1(\sigma_i^+)$. Figs. 16(c)-16(e) illustrate the tipping and tracking behaviour in three-dimension. Three distinct rates are selected for a fixed magnitude $b = 0.37$, each shown in a different colour as mentioned in Fig. 16(a). The rates r_1 and r_3 lie within tracking regions, while r_2 lies in the tipping region. Consequently, the trajectories in Fig. 16(c) and 16(f) follow the same stable limit cycle $\Gamma_2(\sigma_i^+)$, while the trajectory in Fig. 16(d) tips to an alternative stable limit cycle $\Gamma_1(\sigma_i^+)$. Fig. 16(b) shows non-monotone shifts corresponding to different rates.

The impact of varying t_c values on the tipping diagrams is shown in Fig. 17(a) and Fig. 17(b) with the incremental value of 15. The half-bounded tipping regions correspond to monotone input

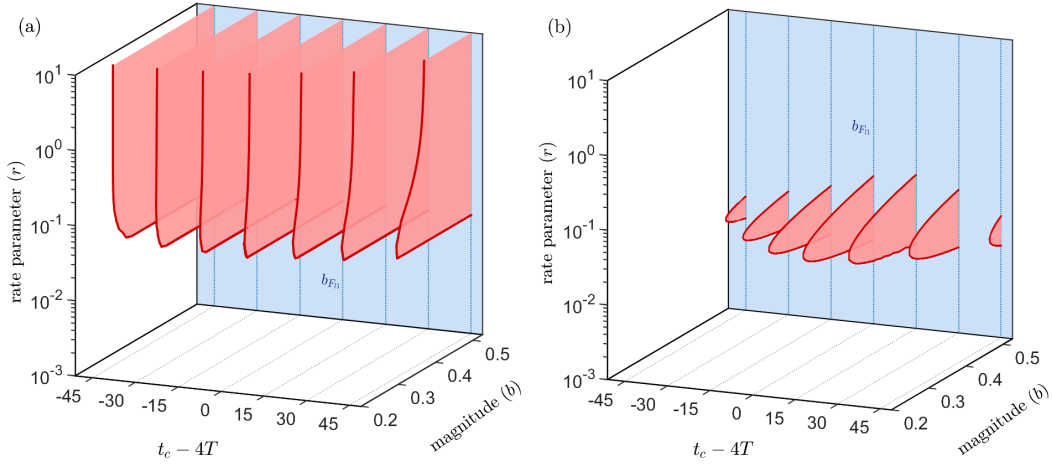


Figure 17. The set of three-dimensional tipping diagrams of the Decroly-Goldbeter glycolysis model (4) with variations in the parameters (t_c vs. b vs. r) of (a) monotone input (7) and (b) non-monotone input (8) for different values of t_c starting from $4T - 45$ to $4T + 45$ in the interval of 15. The blue plane denotes the fold point $b_{F_{11}}$.

(7) and gradually decrease in size as t_c varies. In the case of non-monotone input, unlike the tipping diagram correspond to the van der Pol model in Fig. 11(a), for a fixed value of $t_c = 4T$, the tipping diagram in glycolysis model with non-monotone shift (8) has a single bounded region. Upon varying the values of t_c , Fig. 17(b) illustrates the change in the size of the tipping region.

4.3 General relationship between phase and pace (rate)

While we have discussed the concept of RP-tipping for a fixed initial condition on the base stable limit cycle, it is crucial to examine the relationship between the rate of external inputs and all initial conditions concerning the phase of the base stable limit cycles. This section explores this relationship through Figs. 18 and 19. We begin by discussing this in the context of both models (2) and (4) with a monotone input (7). Fig. 18(a) illustrates the relationship between the rate parameter r and the phase φ_{γ_t} of the stable limit cycle $\Gamma_1(\mu^+)$ in the birhythmic van der Pol model. The figure shows two distinct regions corresponding to tipping phases (blue) and basin unstable (BI) phases (grey). Due to the symmetry of the limit cycle, these regions are repeated twice. As $r \rightarrow \infty$, the monotone input steepens significantly, approaching a step function, which results in the convergence of tipping and basin unstable phases. To further illustrate this, we consider a fixed rate $r = 9$. Fig. 18(b) displays the base limit cycle $\Gamma_1(\mu^+)$, highlighting two sets of phases concerning tipping (blue) and basin instability (grey).

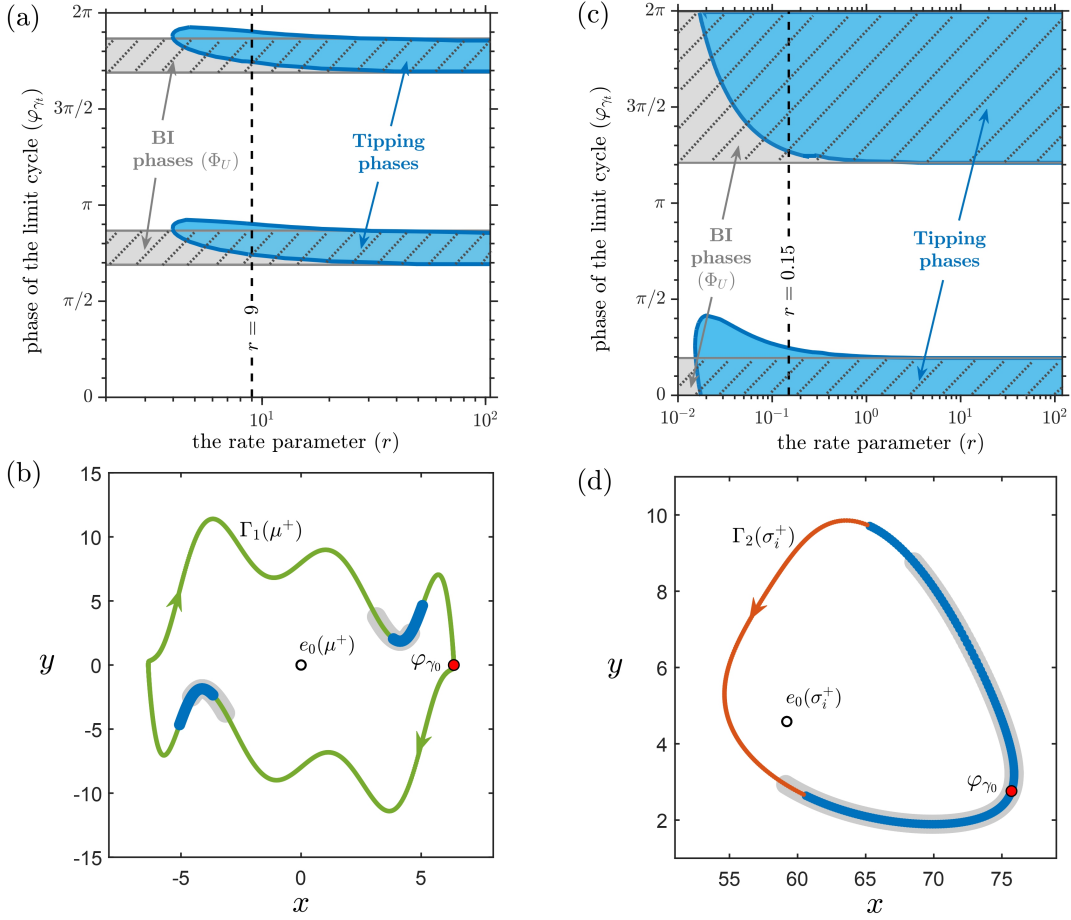


Figure 18. (a) Pace versus phase for the birhythmic van der Pol model (2) with monotone time-dependent external input $\mu(rt)$ (7). The blue region denotes the tipping phases, and the overlapping grey-shaded region denotes basin unstable phases (*BI*). (b) Phase portrait of large amplitude base stable limit cycle Γ_1 at $\mu^+ = 1.52$ with *BI* phases Φ_U (grey) and tipping phases (blue) correspond to the rate value $r = 9$ (see the black dashed line in (a)). (c) Describes the same as (a) for the Decroly-Goldbeter glycolysis model (4) with a monotone input $\sigma_i(rt)$ (7). (d) Small-amplitude base stable limit cycle Γ_2 at $\sigma_i^+ = 1.226$ with basin unstable Φ_U (grey) and tipping phases (blue) for the rate $r = 0.15$ (see the black dashed line in (c)).

Similarly, for higher values of the rate of an input r , Fig. 18(c) illustrates the alignment of tipping phases (blue) with basin unstable phases (grey) of the base limit cycle $\Gamma_2(\sigma_i^+)$ in the glycolysis model. The fragmentation of the regions is due to the position of the initial phase φ_{γ_0} . Fig. 18(d) demonstrates the phase portrait corresponding to Fig. 18(c) for $r = 0.15$, showing the distribution of tipping and *BI* phases along the base limit cycle $\Gamma_2(\sigma_i^+)$.

For the non-monotone input (8), tipping phases and *BI* phases of the base limit cycle exhibit distinct characteristics in each of the models. Unlike the monotone case, these phases do not overlap as $r \rightarrow \infty$; instead, the tipping phases terminate at a finite rate value. This occurs due

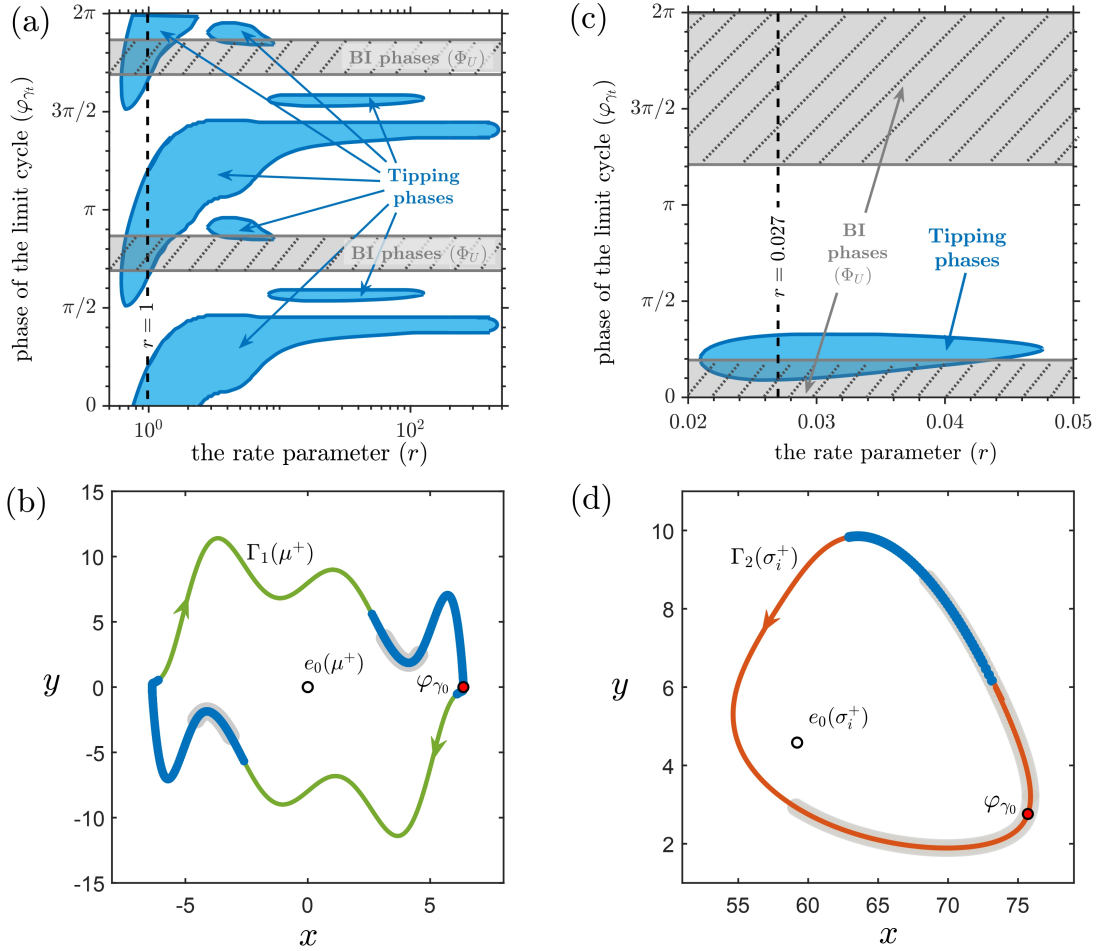


Figure 19. (a) Pace versus phase for the birhythmic van der Pol model (2) with non-monotone time-dependent external input $\mu(rt)$ (8). The blue region denotes the tipping phases, and the grey-shaded region denotes basin unstable phases (BI). (b) Phase portrait of large amplitude base stable limit cycle Γ_1 at $\mu^+ = 1.52$ with BI phases Φ_U (grey) and tipping phases (blue) correspond to the rate value $r = 1$ (see the black dashed curve in (a)). (c) describes the same as (a) for the Decroly-Goldbeter glycolysis model (4) with a non-monotone input $\sigma_i(rt)$ (8). (d) Small-amplitude base stable limit cycle Γ_2 at $\sigma_i^+ = 1.226$ with basin unstable Φ_U (grey) and tipping phases (blue) for the rate $r = 0.027$ (see the black dashed curve in (c)).

to the same asymptotic limit of the non-monotone input in both directions. For a higher rate, the peak of the input undergoes a sharp transition and then quickly returns, creating the impression that there was no transition. Fig. 19(a) shows the fragmented regions of tipping phases (blue) and a constant strip of BI phases (grey) of the base stable limit cycle $\Gamma_1(\mu^+)$ in the birhythmic van der Pol model. The shaded regions repeat due to the symmetry of the limit cycle Γ_1 . Fig. 19(b) presents the base limit cycle $\Gamma_1(\mu^+)$, illustrating two sets of phases related to tipping (blue) and basin instability (grey) for $r = 1$. Similarly, for the Decroly-Goldbeter glycolysis model, Fig. 19(c) depicts the tipping and BI phases. Compared to Fig. 19(a), the blue-shaded region here is smaller,

constrained between 0.02 and 0.05 rate values. For $r = 0.027$, Fig. 19(d) exhibits the phase portrait corresponding to Fig. 19(c), illustrating the distribution of tipping and BI phases along the base limit cycle $\Gamma_2(\sigma_i^+)$. Intuitively, the observed discrepancy between the (blue) tipping phases and the (grey) basin unstable phases arises for non-monotone inputs for two reasons. First, RP-tipping can occur from states that are in the basin of attraction but not close enough to the limit cycle, in which case one would need to consider the basin instability of such points. Second, there are so-called rescue events [Alkhayuon et al \(2023\)](#). In such an event, the system moves to the other basin of attraction, but only temporarily, because rapid trend reversal in the input pushes the system back to the initial basin of attraction and prevents tipping.

5 Conclusions

Owing to the significance of evaluating a threshold in the form of a critical rate of parameters for a sudden collapse in a system state in various real-world systems, research and studies on rate-induced critical transitions are blooming over the current period. In this work, we analysed two distinct birhythmic systems of different nonlinear structures with time-varying external inputs to study RP-tipping between two stable limit cycles, crossing an unstable limit cycle that acts as a basin boundary separating the basin of attraction for both the stable limit cycles. Since the limit cycles are the primary source for the rate-induced phase-tipping, it is essential to define the phase. Due to non-uniformity in the shape of the limit cycle in the birhythmic van der Pol model, unlike the glycolysis model, we defined the phase of the limit cycle using the time instances of the system on the limit cycle. RP-tipping happens not from every phase on the limit cycle but from certain phases depending on the rate r of external input. We considered two types of parameter shifts - monotone and non-monotone - of the chosen parameters in both models to vary over time. We numerically investigated the existence of RP-tipping using two-dimensional tipping diagrams with the parameters in the shift - magnitude and rate - fixing the value of the parameter t_c . To make our results robust, we used the concept of partial basin instability of the limit cycle $\Gamma(p)$ on the fixed-in-time input parameters along a parameter path Δ_p , which is a set-theoretic property of the autonomous frozen birhythmic systems. It is proposed that if $\Gamma(p)$ is partially basin unstable on a parameter path Δ_p , then there exists a parameter setting on Δ_p which assures RP-tipping crossing the critical rate. We presented the partial basin instability of Γ_1 in the birhythmic van der Pol

model and Γ_2 in the glycolysis for our investigation on RP-tipping.

The most challenging component of partial basin instability of $\Gamma(p)$ and RP-tipping is determining the suitable parameter path Δ_p on which the shifts evolve with respect to time. It is not necessary to have partial basin instability of $\Gamma(p)$ with the randomly chosen parameter paths. Choosing the direction of drift of the parameters on Δ_p is also as important as choosing the parameter path. In our case, for both models, we decreased the parameters from p^+ to p^- to witness the basin instability. To distinguish the parameter paths on the birhythmic region of two-parameter bifurcation diagrams, for the birhythmic van der Pol model, the path is chosen vertically, parallel to μ -axis with fixed d whereas, for the glycolysis model, the parameter path is chosen diagonally by changing both the substrate input v and the maximal rate of recycling of the product σ_i in a straight line. However, one may determine other parameter paths. Further, in the birhythmic van der Pol model for a longer parameter path and a fixed rate, we illustrated a series of RP-tipping between limit cycles using a distinct non-monotone input in the form of impulse. At last, the relationship between tipping phases and basin unstable phases is studied using the pace versus phase diagrams for the forcings in both models.

Taking into account various real-life scenarios, it is becoming apparent that R-tipping is just as crucial as B-tipping. It is of the utmost importance to develop alternative techniques, like early warning signals for different B-tippings, to forecast the occurrence of R-tipping, and then RP-tipping. It is also important to verify R-tipping in models with diverse potential dynamics ([Ashwin and Newman 2021](#)). Considering nonlinear models with the coexistence of chaotic attractors for R-tipping will also be quite interesting to study. This present analysis can be made more general by developing the concepts of basin instability and determining the phases for the chaotic attractors.

Data accessibility.

The article has no additional data.

Supplementary material is available online:

(https://github.com/RaviKumarK97/Electronic_supplementary_RP-tipping).

Declaration of AI use.

We have not used AI-assisted technologies in creating this article.

Authors' contributions.

All authors contributed equally.

All authors gave final approval for publication and agreed to be held accountable for the work performed therein.

Conflict of interest declaration.

We declare we have no competing interests.

Funding.

Ravi Kumar K has received funding from IIT Ropar.

Acknowledgments.

P.S.D. acknowledges financial support from the Science & Engineering Research Board (SERB), Government of India (Grant number: CRG/2022/002788).

References

- Alkhayuon H, Tyson RC, Wieczorek S (2021) Phase tipping: how cyclic ecosystems respond to contemporary climate. *Proceedings of the Royal Society A: Mathematical, Physical and Engineering Sciences* 477(2254):20210,059
- Alkhayuon H, Marley J, Wieczorek S, Tyson RC (2023) Stochastic resonance in climate reddening increases the risk of cyclic ecosystem extinction via phase-tipping. *Global Change Biology* 29:3347–3363
- Alkhayuon HM, Ashwin P (2018) Rate-induced tipping from periodic attractors: Partial tipping and connecting orbits. *Chaos: An Interdisciplinary Journal of Nonlinear Science* 28(3)
- Anagnostopoulou V, Pötzsche C, Rasmussen M (2023) *Nonautonomous Bifurcation Theory: Concepts and Tools*. Springer Nature
- Ashwin P, Newman J (2021) Physical invariant measures and tipping probabilities for chaotic attractors of asymptotically autonomous systems. *The European Physical Journal Special Topics* 230(16):3235–3248

- Ashwin P, Wieczorek S, Vitolo R, Cox P (2012) Tipping points in open systems: bifurcation, noise-induced and rate-dependent examples in the climate system. *Philosophical Transactions of the Royal Society A: Mathematical, Physical and Engineering Sciences* 370(1962):1166–1184
- Ashwin P, Perryman C, Wieczorek S (2017) Parameter shifts for nonautonomous systems in low dimension: bifurcation-and rate-induced tipping. *Nonlinearity* 30(6):2185
- Bastiaansen R, Dijkstra HA, von der Heydt AS (2022) Fragmented tipping in a spatially heterogeneous world. *Environmental Research Letters* 17(4):045,006
- Biswas D, Banerjee T, Kurths J (2016) Control of birhythmicity through conjugate self-feedback: Theory and experiment. *Physical Review E* 94(4):042,226
- van der Bolt B, van Nes EH (2021) Understanding the critical rate of environmental change for ecosystems, cyanobacteria as an example. *Plos One* 16(6):e0253,003
- Carpenter SR, Cole JJ, Pace ML, Batt R, Brock WA, Cline T, Coloso J, Hodgson JR, Kitchell JF, Seekell DA, et al (2011) Early warnings of regime shifts: a whole-ecosystem experiment. *Science* 332(6033):1079–1082
- Chaparro-Pedraza PC (2021) Fast environmental change and eco-evolutionary feedbacks can drive regime shifts in ecosystems before tipping points are crossed. *Proceedings of the Royal Society B* 288(1955):20211,192
- Dakos V, Bascompte J (2014) Critical slowing down as early warning for the onset of collapse in mutualistic communities. *Proceedings of the National Academy of Sciences USA* 111(49):17,546–17,551
- Dueñas J, Núñez C, Obaya R (2023) Critical transitions in d-concave nonautonomous scalar ordinary differential equations appearing in population dynamics. *SIAM Journal on Applied Dynamical Systems* 22(4):2649–2692
- Ermentrout B (2002) *Simulating, Analyzing, and Animating Dynamical Systems*. Society for Industrial and Applied Mathematics

- Ghil M, Sciamarella D (2023) Dynamical systems, algebraic topology, and the climate sciences. EGU sphere pp 1–53
- Gladwell M (2000) The tipping point: How little things can make a big difference. Little, Brown
- Goldbeter A (1996) Biochemical Oscillations and Cellular Rhythms: The Molecular Bases of Periodic and Chaotic Behaviour. Cambridge University Press
- Halekotte L, Feudel U (2020) Minimal fatal shocks in multistable complex networks. Scientific Reports 10(1):11,783
- Hasan CR, Cárthaigh RM, Wieczorek S (2023) Rate-induced tipping in heterogeneous reaction-diffusion systems: an invariant manifold framework and geographically shifting ecosystems. SIAM Journal on Applied Dynamical Systems 22(4):2991–3024
- Kaiser F, Eichwald C (1991) Bifurcation structure of a driven, multi-limit-cycle van der pol oscillator (i): The superharmonic resonance structure. International Journal of Bifurcation and Chaos 1(02):485–491
- Kaur T, Dutta PS (2022) Critical rates of climate warming and abrupt collapse of ecosystems. Proceedings of the Royal Society A: Mathematical, Physical and Engineering Sciences 478(2264):20220,086
- Keane A, Krauskopf B, Lenton TM (2020) Signatures consistent with multifrequency tipping in the atlantic meridional overturning circulation. Physical Review Letters 125:228,701
- Kloeden PE, Rasmussen M (2011) Nonautonomous dynamical systems. 176, American Mathematical Soc.
- Kwuimy CK, Nataraj C (2015) Recurrence and joint recurrence analysis of multiple attractors energy harvesting system. In: Structural Nonlinear Dynamics and Diagnosis: Selected papers from CSNDD 2012 and CSNDD 2014, Springer, pp 97–123
- Lenton TM, Held H, Kriegler E, Hall JW, Lucht W, Rahmstorf S, Schellnhuber HJ (2008) Tipping elements in the earth’s climate system. Proceedings of the National Academy of Sciences USA 105(6):1786–1793

- Longo IP, Núñez C, Obaya R, Rasmussen M (2021) Rate-induced tipping and saddle-node bifurcation for quadratic differential equations with nonautonomous asymptotic dynamics. *SIAM Journal on Applied Dynamical Systems* 20(1):500–540
- Longo IP, Núñez C, Obaya R (2024) Critical transitions in piecewise uniformly continuous concave quadratic ordinary differential equations. *Journal of Dynamics and Differential Equations* 36(3):2153–2192
- Mickens RE (1996) *Oscillations in planar dynamic systems*, vol 37. World Scientific
- Monod J, Wyman J, Changeux JP (1965) On the nature of allosteric transitions: a plausible model. *Journal of molecular biology* 12(1):88–118
- Moran F, Goldbeter A (1984) Onset of birhythmicity in a regulated biochemical system. *Biophysical chemistry* 20(1-2):149–156
- Nakao H (2016) Phase reduction approach to synchronisation of nonlinear oscillators. *Contemporary Physics* 57(2):188–214
- O’Keeffe PE, Wieczorek S (2020) Tipping phenomena and points of no return in ecosystems: beyond classical bifurcations. *SIAM Journal on Applied Dynamical Systems* 19(4):2371–2402
- O’Brien DA, Deb S, Gal G, Thackeray SJ, Dutta PS, Matsuzaki SiS, May L, Clements CF (2023) Early warning signals have limited applicability to empirical lake data. *Nature Communications* 14(1):7942
- O’Sullivan E, Mulchrone K, Wieczorek S (2023) Rate-induced tipping to metastable zombie fires. *Proceedings of the Royal Society A: Mathematical, Physical and Engineering Sciences* 479(2275):20220,647
- Ritchie PD, Clarke JJ, Cox PM, Huntingford C (2021) Overshooting tipping point thresholds in a changing climate. *Nature* 592(7855):517–523
- Ritchie PD, Alkhayouon H, Cox PM, Wieczorek S (2023) Rate-induced tipping in natural and human systems. *Earth System Dynamics* 14(3):669–683

- Sarkar S, Sinha SK, Levine H, Jolly MK, Dutta PS (2019) Anticipating critical transitions in epithelial–hybrid-mesenchymal cell-fate determination. *Proceedings of the National Academy of Sciences USA* 116(52):26,343–26,352
- Scheffer M (2009) *Critical Transitions in Nature and Society*. Princeton Studies in Complexity, Princeton University Press
- Scheffer M, Carpenter S, Foley JA, Folke C, Walker B (2001) Catastrophic shifts in ecosystems. *Nature* 413(6856):591–596
- Trefois C, Antony PM, Goncalves J, Skupin A, Balling R (2015) Critical transitions in chronic disease: transferring concepts from ecology to systems medicine. *Current opinion in biotechnology* 34:48–55
- Vanselow A, Halekotte L, Feudel U (2022) Evolutionary rescue can prevent rate-induced tipping. *Theoretical Ecology* 15(1):29–50
- Vanselow A, Halekotte L, Pal P, Wieczorek S, Feudel U (2024) Rate-induced tipping can trigger plankton blooms. *Theoretical Ecology* 17:89–105
- Wieczorek S, Ashwin P, Luke CM, Cox PM (2011) Excitability in ramped systems: the compost-bomb instability. *Proceedings of the Royal Society A: Mathematical, Physical and Engineering Sciences* 467(2129):1243–1269
- Wieczorek S, Xie C, Jones CK (2021) Compactification for asymptotically autonomous dynamical systems: theory, applications and invariant manifolds. *Nonlinearity* 34(5):2970
- Wieczorek S, Xie C, Ashwin P (2023) Rate-induced tipping: Thresholds, edge states and connecting orbits. *Nonlinearity* 36(6):3238
- Zhang W, Xu W, Niu L, Tang Y (2023) Bifurcations analysis of a multiple attractors energy harvesting system with fractional derivative damping under random excitation. *Communications in Nonlinear Science and Numerical Simulation* 118:107,069